Title
THERMODYNAMIC STABILITY OF CERTAIN INTERMETALLIC COMPOUNDS MADE FROM TRANSITION ELEMENTS

Author
Wengert, Paul R.

Publication Date
1969-04-01

UCRL-18727

THERMODYNAMIC STABILITY OF CERTAIN INTERMETALLIC COMPOUNDS MADE FROM TRANSITION ELEMENTS

Paul Richard Wengert
(Ph. D. Thesis)

April 1969

AEC Contract No. W-7405-eng-48

LAWRENCE RADIATION LABORATORY
UNIVERSITY of CALIFORNIA BERKELEY

UCRL-18727

DISCLAIMER

TABLE OF CONTENTS

THERMODYNAMIC STABILITY OF CERTAIN INTERMETALLIC BINARY COMPOUNDS MADE FROM TRANSITION ELEMENTS

Paul R. Wengert

Inorganic Materials Research Division, Lawrence Radiation Laboratory
and Department of Chemistry, University of California
Berkeley, California

ABSTRACT

The Zr compounds of Re, Ru, Os, Rh, Ir, Pd, Pt, Ag, and Au are studied. Limits and estimates of the Gibbs free energy of formation of these compounds are determined by observing high temperature reactions of C and ZrC with the above elements and with their Zr compounds. $ZrRh_3$, $ZrIr_3$, $ZrPd_3$, and $ZrPt_3$ exist in equilibrium with C and ZrC and have $\Delta F^\circ < -11.5$ kcal/g-atom of compound calculated at 298°K. C and ZrC exist in equilibrium with the Ru (0.75 at.% Zr), Os ($\leq$ 0.06 at.% Zr), Ag (liquid, $\leq$ 0.05 at.% Zr), and Au (liquid, 9.5 ± 3.5 at.% Zr) phases at 1500°C. The ΔF°_f ($ZrRu_2$) is calculated from the equilibrium data to be -13.6 ± 0.9 kcal/g-atom at 1500°C and ΔF°_f ($ZrAu_4$) is calculated to be -7.93 ± 0.35 kcal/g-atom at 1000°C. The activity coefficients of Zr (γ_{Zr}) in the limit of 0% Zr are calculated from the three phase equilibria. No ternary compounds were observed for the above systems. In the case of the C-Zr-Re system, a molar ratio of Zr to Re of 19.0 to 81.0 was found in the hcp Re phase in the presence of C and ZrC indicating that this phase extended into the ternary system; therefore, no thermodynamic information could be determinded by this method for the Zr-Re binary system. The lattice parameters of the expanded hcp Re phase are determined: $a = 2.7810 \pm 0.0004$Å, $C = 4.4590 \pm 0.0008$Å. Miscellaneous propoerties of the binary alloys are given.

Reactions of carbides, borides and nitrides with transition elements

reported by other authors are reviewed. Limits on ΔF°_{f} of the following compounds are calculated at 298°K : $ZrRh_3$, $ZrIr_3$, $HfRh_3$, $HfIr_3$, $ThIr_2$, $ThRh_2$, $ThAu_3$, $NbPt_3$, $NbIr_3$, $NbRe_{3\pm x}$, $TaPt_3$, UIr_3, URh_3, U_2IrC_2, U_2RhC_2, and UAu_3.

An appendix on the Engel and Brewer concepts of crystal structure and bonding is included.

I. INTRODUCTION

Some intertransition element compounds have been predicted to be very stable compared to more common metallic compounds.[2,4] Leo Brewer[1-5*] supporting the earlier work of Neils Engel[6] has shown that these compounds have d electron bonds as well as s electron and p electron bonds. Just as there is a driving force to form an octet of bonded electrons when only s and p electrons are available, as in BN, there is also a driving force to use the additional five d electron bonds when they are available. With d electron bonds as well as s and p electron bonds, some of the intertransition element compounds would be expected to be very stable. The following experimental work confirms this stability. The 4d and 5d transition series were chosen for this study because the d electrons of Period Six elements have larger bonding energies than those of the corresponding Period Four element.[1] The high stability coupled with the high melting points found in some of the compounds would lend them desirable for high temperature applications.

In the field of thermodyanmics, the stability of a compound is synonomous with the Gibbs free energy of formation (ΔF_f) of the compound and with the activity coefficients (γ_i) of the various elements making the compound. This information is obtained for the Zr binary compounds of Ru, Os, Rh, Ir, Pd, Pt, Ag and Au from the ternary phase diagrams of C, Zr, and one of the aforementioned elements. Graphite is chosen as a

---

*References 1-9 represent articles written to date on the Engel Correlation and the corresponding predictions made by Leo Brewer. Appendix A also discusses these concepts.

third constituent because the Gibbs free energy of the formation of ZrC, ΔF_f° (ZrC), has been determined[10] and because the binary systems of graphite with the other elements has been determined. The C-Zr-Re ternary phase diagram is also discussed.

The d electron bonding in transition element compounds can be illustrated by the example of s and p electron bonding in ammonia boron trifluoride:

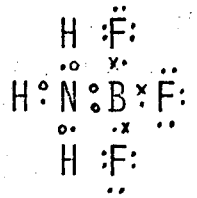

The circles refer to valence electrons contributed by N, the x's refer to electrons contributed by B, and the dots refer to those contributed by H and F. The B-F and the N-H bonds are formed by one electron from each atom; there is no formal charge transfer. The B-N bond is different; the electron pair remaining on N after all of the H's are bonded is shared with the B vacant orbital. There is a formal charge transfer of 1 from the N atom to the B atom. The formal charge transfer is such that B and N each attain the C valence electron configuration of (s^1p^3), that is, they both attain the stable configuration of the half-filled valence electron orbital.

The d electron bonding of $ZrIr_3$ is similar. In the elemental solids the Engel Correlation in its simplest form suggests the following electronic configuration: Zr (hcp, $d^2s^1p^1$) and Ir (fcc, $d^6s^1p^2$). Zr (hcp) has four bonding electrons per atom. The Ir (fcc) structure has seven bonding electrons per atom: one s bonding electron, two p bonding electrons, and four d bonding electrons because two of the d electrons are paired internally. There are a total of 25 bonding electrons in one Zr and three Ir atoms.

When the $ZrIr_3$ fcc structure is formed, the Engel Correlation predicts three s and p bonding electrons per atom giving Zr a ($d^1s^1p^2$) electronic configuration without considering electron transfer. The Zr can bond its one d electron and three s and p electrons to Ir atoms in a manner similar to the B-F and N-H bonds. If the d electron internal pairs of the Ir atoms were shared with the Zr low-lying vacant d orbitals, then the number bonding d electrons would increase by six. The three bonds formed by the six bonding electrons would be similar to the B-N bond of H_3NBF_3. Zr would assume a formal charge of -3 and Ir would assume a formal charge of + 1. The valence electron configurations would be Zr^{-3} ($d^4s^1p^2$) and Ir^{+1} ($d^5s^1p^2$). The total bonding electrons in $ZrIr_3$ is 31. From the reaction: $Zr(hcp) + Ir(fcc) \rightarrow ZrIr_3(fcc)$, one can see that there is a gain of six bonding electrons in the formation of $ZrIr_3$ or a change of 1.5 bonding electrons/atom. It is this change in bonding that suggests a large negative value of ΔF_f° ($ZrIr_3$) reflecting its high stability.

In the formation of $ZrIr_3$, the additional bonding is attained because electron pairs are shared with vacant d orbitals. An increase in the number of bonding electrons when a transition element compound is formed from its elements can only come about if one element has vacant d orbitals and the other element has internal electron pairs to share. Groups 6 and 7 (i.e. W and Re) already possess the stable valence electron configuration of half-filled energy levels. When elements to the left of Group 6 are alloyed with elements to the right of Group 7, an increase in stability reflecting the increase in the number of d bonding electrons on compound formation is expected. When elements to the left of Group 6 are alloyed among themselves, there is no electron pair sharing, and no increase in the number of bonding electrons is expected. The same

argument is true when elements to the right of Group 7 are interalloyed. The result is that these alloys would not exhibit large negative Gibbs free energies of formation, as is expected for $ZrIr_3$. Other compounds that are expected to exhibit high stability are alloys of Y, La, Zr, Hf, Nb and Ta with Ru, Os, Rh, Ir, Pd, and Pt, Ag, and Au.

For a given element on the left of the transition series, Zr as an example, the number of bonding electrons formed in alloying the elements increases as the atomic number of the other element increases from Os to the right of the Periodic Table. The internal pressure of the elements decreases after Os reaching that of Zr at Pt. The stability of the internally paired d electrons also increases with atomic number after Os. Considering these variables, a peak in the stability of Zr compounds is expected near Ir and Pt. The same argument can be applied to the Zr alloys of Ru through Ag. It is this expected trend in stability that is experimentally investigated.

II. GENERAL EXPERIMENTAL PROCEDURE

To determine the desired ternary phase diagrams, both solid state and liquid state reactions were run. The reactants for the solid state reactions varied: ZrC was hot pressed with Ru, Os, Rh, Ir, Pd, Pt, Ag, or Au; C and ZrC were heated with each of the above elements; and Zr alloys of Re, Ru, Os, Ag, and Au were heated with C. Liquid Ag, Au and their Zr alloys, ZrAg and $ZrAu_3$ and $ZrAu_4$, were reacted with solid C and ZrC. The desired result was to pin down the three phase region involving C and ZrC; the third phase varied from one alloy system to another.

A. Starting Materials

The starting materials for the solid state reactions were powders of 200-400 mesh. Other materials were used for making the Zr_5Re_{24} binary alloy and for the liquid reactions: Re zone-refined rod of one-eighth inch diameter, Ag sponge of 6 to 14 mesh, and Au sheet 0.005 of an inch thick. The elemental powders were 99.9 wt.% or higher purity with the exceptions of Rh (> 1 wt.% Ir), Pd (~ 1 wt.% Pt), and Zr. The major impurities of the Zr powder reported by the manufacturer were: 0.05 wt.% Fe; 0.1 wt.% O; 0.03 wt.% H; 0.02 wt.% N; < 0.02 wt.% Sn; < 0.01 wt.% Ti, W, and Zn; and 0.005 wt.% Hf. The ZrC powder was reported by the manufacturer to be 98 wt.% pure, but independent spectroanalysis showed 0.5 wt.% Hf as the only impurity. The Ag sponge contained 0.001 wt.% Cu and < 0.001 wt.% Ca. Analysis of the Au sheet showed the major impurities to be 0.02 wt.% Ti, 0.02 wt.% Pd, and 0.015 wt.% Ag. The graphite reactant powder was reported by the manufacturer to be five nines pure. The graphite material used in making the hot press dyes was manufactured by Great Lakes Carbon Company, Sanborn, New York under the trade name of "Graphitite G"; by independent spectroanalysis it was found to contain the following:

0.001 wt.% Cu; $\leq$ 0.001 wt.% Ca and Mg; 0.003 wt.% Al; 0.003 wt.% H, 0.006 wt.% O; and 0.001 wt.% N.

The powders used for the solid state reactions and for the alloy synthesis were mixed by rolling. Milton R. Pickus designed a four vial holder that rotated the vials about their longitudinal and their short axes simultaneously. The powders experienced a compound motion of free fall and shear. As a result powders of different mesh mixed well. A standard ball mill drive rotated the holder. Samples were rolled 48 hours before heating.

B. Furnaces Used

Four types of furnaces were used for the equilibrations. A multi-station hot press was employed in all solid state reactions. As the name implies, a sample can be heated and pressed simultaneously. The hot press chamber is fabricated from stainless steel and is water cooled. A Ta filament made from a 1 inch by 0.005 inch strip and formed into a nearly complete cylinder serves as the heating element. A multilayer Ta radiation shield surrounds the filament. The entire heating unit is mounted on a shaft passing through a Wilson seal so that it can be moved vertically from outside the chamber. The sample dies are fabricated from "Graphitite G." One die consists of two half inch diameter plungers and a sleeve of one inch outside diameter and one-half inch inside diameter. The reactant powders are placed in the die and are hot pressed to a one-half inch diameter, one-eighth inch thick disc. A maximum of eight dies are placed on a lazy susan which can be rotated so that different dies will align with a hydraulic ram used to apply the desired pressure and with the heating assembly. Wilson seals are used for the shaft carrying the lazy susan and for the shaft transmitting the pressure from the hydraulic

ram. The furnace can be used with any oxygen free atmosphere (600 Torr of Ar was chosen) or vacuum. After one pressing is completed, the pressure is released; the heating assembly is raised; the lazy susan is rotated to the next position; the heating assembly is lowered to surround the second die; and the second hot pressing commences.[11] The multi-station hot press was designed by and built under the supervision of Milton R. Pickus for use in the Inorganic Materials Research Division of the Lawrence Radiation Laboratory.

Using the hot press for solid state reactions has a definite advantage. The kinetics of such reactions depends upon the area of contact between the various reactants. By starting with powder and pressing them together while heating, the reaction kinetics are improved. As long as both reactants and products are solids, the reaction equilibrium will not be affected by the use of pressure. The equilibrium depends upon the Gibbs free energy of the reaction, ΔF_{rx}. The change in ΔF_{rx} due to the increase in pressure can be expressed as: $\Delta F_{rx,\ 500\ atm.} - \Delta F_{rx,\ 1\ atm.} = \int_1^{500} \Delta V_{rx}\, dP$. The difference in volume between products and reactants (ΔV_{rx}) is small because they are both solids and the associated difference in ΔF_{rx}'s is not expected to exceed ± 200 calories, a small change compared to the kilocalorie values of the free energies of formation of the products and reactants. As a result, the reactions that take place under pressure are also expected to occur at one atmosphere. The kinetics of the reaction are improved, however, and less time is necessary before the reaction products are observed.

A vacuum furnace with a Ta sheet or a W mesh filament was used for the binary alloy homogenization and for the melting point determinations.

Difficulty was encountered in running the hot press for long periods of time and the vacuum furnace was also used to supplement the hot press runs. After initial hot pressing the samples were compact and the powder particles were in good contact with each other. Both vacuum and 600 Torr of He were used. The furnace and crucible were baked out before runs and the sample weight losses were carefully watched.

An arc furnace with a water cooled copper crucible was used to initially melt the binary alloys. Thirty gram samples of cold pressed powder, or rod in the case of Re, were melted into buttons, flipped, and remelted five times. A Zr button was used as a getter to purify the 700 Torr Ar atmosphere.

An induction furnace was used for the liquid reactions of the Ag and Au ternary systems. The fields generated stir metal liquid and improve reaction kinetics. The crucible made of 'Graphitite G' was placed inside a vertical quartz tube. After pumping on the chamber for 2 to 3 hours, He was passed from the top to the bottom of the tube and bubbled through a trap filled with diffusion pump oil to keep the gas flow one way. A water cooled copper coil surrounding the outside of the quartz tube served as a heating source.

Temperature readings were taken with an optical pyrometer. The readings reported are the average of the filament fading temperatures from high and low temperature approaches. The average correction for the quartz furnace windows was found to be +15°C in the 1500°C temperature range. The error assigned to the readings is the spread in the temperature readings over the duration of the heating. Other sources of error are ±10°C associated with eye accuracy and ±3°C for the uncertainty of the calibrations of the window and of the pyrometer. Readings

were taken off of the top of the crucibles perpendicular to the radiating filament so that black body radiation was more closely approached. When a crucible lid was not employed, temperature readings were taken from a corner inside the crucible.

C. Methods of Analysis

X-ray diffraction, metallography, and electron microprobe analysis were used to determine the reaction products. The product phases were identified with a Pickert Model No. 3488K diffractometer. Lattice parameters were usually determined to three significant figures. Such an accuracy was considered sufficient to make sure that all of the observed peaks were accounted for. Greater accuracy was not considered necessary because the variation of the lattice parameter of the various phases has not been determined as a function of the other components of the ternary systems present. The fixed horizontal sample holder made it very easy to x-ray the powder samples. Comparison of the products' x-ray pattern to that of the reactants made the identification of peaks easier. All of the phases observed had been reported previously as indicated in Table VI.

Metallography was straightforward; no etching was necessary. For all of the samples with the exception of those containing Ag and Au, polishing with one micron diamond paste and kerosene on a canvas wheel was enough to polish the sample and leave a visible difference between the phases. In the case of samples containing Ag and Au using six micron diamond paste and kerosene on a canvas wheel intermittently with 0.05 micron alumina and kerosene on a felt wheel produced distinguishable phases.

A Materials Analysis Company Model 400 electron microprobe analyzer was used to determine the concentration of Zr present in the elemental phases of Re, Ru, Os, Ag, and Au. In the microprobe a tungsten filament furnishes electrons which are focused and accelerated to the sample. The accelerating potential selected for the present work is 20 kilovolts. A beam of 1 to 2 microns diameter is claimed by the manufacturer. The electrons excite the characteristic x-rays of the elements present in the sample. The characteristic x-rays are picked up by any one of three spectrometers, each one tuned for a particular element present in the sample. The signal intensity from a spectrometer is fed through a pulse height analyzer and read out on a scaler. The working principle of the apparatus is similar to an x-ray diffractometer; the sample in the microprobe is equivalent to the target in the x-ray tube of the diffractometer, and the target in the diffractometer is similar to the analyzing crystal in the microprobe.

The L_α characteristic x-ray of Zr at 6.070Å was detected by a spectrometer using a PET (pentaerythritol) single crystal [$(hk\ell) = (002)$; $2d = 8.742$Å] and a Xe sealed proportional spectrometer. The specimen current used was in the 350 milliamp range. The intensity from a 100% pure Zr standard was on the order of 10,000 to 15,000 counts per 10 seconds. Data were taken as a group of twenty readings counting for 10 seconds each or as a group of ten readings counting for 20 seconds each. The ratio of the sample to standard counts is proportional to the wt.% Zr. The concentration of C was not determined. There is difficulty obtaining a quantitative analysis of C with the electron microprobe because its mass is small compared to the other constituents and because the electron beam decomposes the hydrocarbons in the vacuum and C tends to deposit on the sample with time. In all the systems studied, except the C-Zr-Re system,

the C concentration was assumed to be small. The count from the principle element of the phase, i.e. Re, Ru, Os, Ag, or Au, was monitored by another spectrometer to make sure that there was no interference from the ZrC phase present. The weight percent of these elements obtained from the computer program was not considered in the quantitative analysis of Zr, however, because of the ±5% error attributed to microprobe readings. An example will serve the point; consider a phase measuring 98 wt.% Ru. The error associated with this value is ±4.9 wt.%. Therefore, the actual wt.% Ru is between 100 and 93 giving a Zr concentration of 0 to 7 wt.%. On the other hand if the wt.% Zr is determined to be 0.80 wt.%, the associated error is ±0.04 wt.% (±5% of 0.80 wt.%). The wt.% Ru is 99.20 ± 0.04 wt.% and both Zr and Ru weight percents are determined more accurately. The output from the microprobe is automatically fed to a computer key punch and to a typewriter.

The computer program used to analyze the data from the microprobe was the EMX - EMX2 combined program written by J. Z. Frazer, R. W. Fitzgerald, and A. M. Reid of Scripps Institution of Oceanography.[12] The EMX program corrects for dead-time losses; drift, assuming a linear variation with time; and background. The method of input chosen for the background can be selected using this program. Background readings were taken as sets and placed before each appropriate standard set and sample set. The EMX2 program corrects for absorption by combining the works of Philibert, Duncumb and Shields, and Heinrich. The program corrects for K-K fluorescence but not for K-L or L-L fluorescence because of the uncertainty of such calculations. Since the Zr L_α line of 6.070Å was used, fluorescence corrections are not applied to this work. No atomic number corrections are included because of the current difficulties with such corrections. The basic program was adopted for use of the Lawrence Radiation Laboratory's CDC 6600 computer.

The error generally attributed to microporbe analysis using 100% standards and computer corrections is ±2 to ±5 of the amount of the element.[13-15] The EMX - EMX2 program does not calculate the error of the quantitative analysis given. A Zr-Au test standard was made to check the microprobe accuracy independent of the assumed accuracy in the range of the sample concentration. The test standard was analyzed each time a Zr-Au sample was analyzed. The results are given in Table I(a). The dates are presented merely to indicate the spread of time over which the readings were taken. The microprobe was constantly under minor modification. There is a 36% spread in the concentration of Zr from 3.0 ± 3.8 at.% Zr in the Au phase.

A wet chemical analysis was run to check the microprobe results. The test standard was taken into solution and was compared with solutions of known concentration near the concentration of the microprobe test standard. The actual analysis performed by Robert D. Giauque was by x-ray spectrometry using an iodine 125 radioisotope source. The isotope was used to excite x-rays in a target material; the K_α x-rays of Rh were used in the present case. The target x-rays bombarded the sample to produce the characteristic radiation of Zr. The back-scattered x-rays from the Rh were used as an internal standard. A more complete description of the technique appears elsewhere.[16] The analysis showed that the microprobe test standard contained 3.40 ± 0.07 at.% Zr. The average of all the microprobe analyses is 3.35 at.% Zr.

If one analysis of the microprobe were relied upon, the expected error would be ±18% of the actual at.% Zr at this level of Zr concentration. Refering to Table I(a), it can be seen that 50% of the analyses are within the expected ±5% accuracy. The 80% confidence limit of detection given by H.S. deBen[17] occurs at 0.076 at.% Zr. The at.% Zr found in the test

standard at only 50% confidence is well above this value.

The source of error is not obvious. The error cannot be attributed to improper corrections of absorption or fluorescence. Since the average value is in good agreement with the wet analysis, the computer corrections are correct. The $Zr_{3.40}$ $Au_{96.60}$ test standard was found to be homogeneous. The microprobe did appear to be quite sensitive to the W filament alignment, and the misalignment of a filament represents the type of drift which is not linear but is more quantum in nature. If the random error were associated with the drifting filament alignment, the Zr standard counts at the beginning of the run (ST) would be expected to differ from the Zr standard counts taken at the end of the run to correct for linear drift (STD). Table I(a) gives the maximum deviations in the individual counts between the ST and STD readings expressed in terms of the standard deviation. A check to see if all of the readings from the two groups of counts differed by more than three times the standard deviation associated with statistical counts (3σ) showed no correlation to the error in at. % Zr for the various runs. The computer program is designed to reject ST and STD data groups if an individual reading within that group varies from the average by more than 3σ. Although the error cannot be explained by the filament alignment, it would probably be good practice to make sure that all standard counts, ST and STD, agree within 5σ.

The error could possibly have been reduced by making sure that the total counts from the sample for the element to be analyzed added to a specific value. Such a practice would improve the statistics. Each analysis of the microprobe test standard represents a total Zr count of 5,000 counts. The 3σ deviation is $\pm$ 4.2% or 210 counts. Using a 100% Zr standard count of 30,000 counts as a base, the associated error would be

±0.13 at.% Zr or 3.9% of the 3.40 at.% Zr true value. This calculation implies that there is a 99% statistical probablity of finding the at.% Zr within ±3.9% of the 3.40 (±0.07) at.% Zr value. Statistical error alone can not account for the ±18% error observed. The total Zr counts off of the test standard for all analyses is 23,390 and the average at Zr is 3.35 at%. The error associated with this count, using the 100% Zr standard base as before, is ±0.04 at.% Zr or ±1.2% of the amount present. Since the overall average agrees well with the wet analysis, it is possible that an increased total count may have improved the statistics; however, it must be remembered that this is only one such count and the first count of 5,000 (3.47 at.% Zr analysis) also agrees well with the wet analysis.

In summary, the above analysis shows that the present work associated with Zr-Au samples in the 3 at.% Zr range is in error by ±18% of the actual value. Making sure that the total sample counts add to 25,000 counts and that all 100% standard counts (ST and STD) of an element agree with each other to within 5σ may decrease the error. The results of the study of the $Zr_{3.40}$ $Au_{96.60}$ test standard showed that an error of ±5% cannot be automatically assumed and that making test standards in the composition range of the alloy system of interest is a necessary step if any error limits are to be attributed to the quantitative analysis.

D. Superconductivity Measurements

The following compounds were checked for superconductivity: ZrRu, $ZrOs_2$, $ZrIr_3$, ZrAg, and $ZrAu_3$ + $ZrAu_4$ (two phase sample). The mutual inductance of two coaxial coils containing one of the samples was measured. The change in magnetic susceptibility was observed as a function of temperature. No change was observed between 1.4 and 18°K indicating that the

samples were not superconducting or ferromagnetic in this temperature range. The method used is covered in greater detail by Eckhard Nembach.[18]

This concludes the description of the general procedures and pieces of equipment used. More detailed procedures varied with each systems studied. They will be discussed later.

III. THERMODYNAMIC DATA FROM TERNARY PHASE DIAGRAMS

From the experimental evidence of which phases exist in equilibrium with each other, ternary phase diagrams have been determined. Examples of the two types of diagrams found for the systems studied are given in Fig. 1, the C-Zr-Ir System; and Fig. 2, the C-Zr-Ru System. Joins are shown in the diagrams indicating the binary phases which exist in equilibrium. The diagrams are simplified in that no attempt has been made to show solubility limits. Those joins directly observed by reaction are indicated by solid lines; $ZrIr_3$ was found to exist in equilibrium with both ZrC and C. It may be recalled from thermodynamics that two joins cannot cross, for there would then be a four phase equilibrium at the join intersection of the ternary phase diagram with temperature and pressure fixed which is not allowed by the phase rule. With temperature and pressure fixed, the phase rule becomes C-P = F. In the present experimental equilibrations, the number of components (C=3) equals the number of phases (P=3) leaving no degrees of freedom (F=0). Therefore, compounds to the Zr-rich side of $ZrIr_3$ must be in equilibrium with ZrC and alloys to the Ir-rich side must be in equilibrium with C. These possibilities for the Zr-Ir system are indicated in Fig. 1 by the dotted joins. In Fig. 2 the C-ZrC-Ru three phase equilibrium was directly observed indicating that all the binary compounds of Zr and Ru are in equilibrium with ZrC. The above is true if there are no ternary phases present; none were observed in the three phase equilibria represented in Figs. 1 and 2.

If temperature and pressure are not fixed the phase rule is stated as C-P+2 = F. It can be seen that as many as five phases may be found to exist in equilibrium at some point in the five dimensional space represented by the variables of temperature, pressure, and the three mole fractions of the components. The Gibbs free energy of the compounds involved change such a small amount with changes in temperature and pressure that the corresponding ternary diagrams for all C-Zr-M (M ≡ any of the transition elements: Re, Ru, Os, Rh, Ir, Pd, Pt, Ag, or Au) systems may be expected to remain the same throughout the entire solidus region of the diagram, i.e., until the liquid phase is encountered. It is certainly expected to remain the same for the Re, Ru, Os, Rh, Ir, Pd, and Pt systems within ±100°C of the range of experimental observations of this work.

The thermodynamic stability of the compounds of several Zr binary systems presented can be determined from the various ternary phase diagrams experimentally determined. Graphite was chosen as the third constituent for the ternary systems for two reasons: (1) the thermodynamic stability of ZrC, measured by ΔF_f (ZrC), has been determined;[10] and (2) all binary compounds were expected to have a low solubility into the ternary region of the phase diagram and no ternary phases were expected.

A. Calculation of Activity Coefficients From Ternary Phase Diagram

Activity coefficients may be obtained from the ternary phase diagram presented. The C-Zr-Ru phase diagram will serve as an example. The derived activities (a_i) and activity coefficients (γ_i) will be based upon the solvent standard state, i.e. when $x_i = 1$ ($x_i \equiv$ the mole fraction of component i), then $a_i = 1$ and $\gamma_i = 1$. When the C, ZrC, and Ru phases exist in equilibrium, the activity of all the components in the three phases is fixed. The activity of Ru (γ_{Ru}) is close to one since very little Zr(0.75 at.% Zr) and presumably a negligible amount of graphite dissolved into the Ru phase. The activity of graphite (γ_C) is equal to one because of the presence of pure graphite. Since all of the phases are in equilibrium with each other, the activity of each component is the same in all three phases:

$$a_{Ru}^{Ru} = a_{Ru}^{C} = a_{Ru}^{ZrC} \simeq 1$$

$$a_{C}^{C} = a_{C}^{ZrC} = a_{C}^{Ru} = 1$$

$$a_{Zr}^{ZrC} = a_{Zr}^{Ru} = a_{Zr}^{C} = \text{constant}$$

The superscripts designate the phase being discussed; for example, a_{Ru}^{ZrC} represents the activity of Ru in the ZrC phase.

The activity of Zr can be calculated because the ΔF_f° (ZrC) is known; at 1500°C, the ΔF_f° (ZrC) = -42.118 kcal/mole. ΔF_f° (ZrC) may also be expressed as:

$$\Delta F_f^\circ \text{ (ZrC)} = +RT \ln a_C \, a_{Zr}$$

Using the appropriate values:

$$-42.118 \text{ kcal/mole} = R(1773^\circ K) \ln [(1)(a_{Zr})]$$

$$\log a_{Zr} = \frac{-42118}{(2.303)(1.987)(1773)} = -5.191$$

$$a_{Zr} = 10^{-5.191}$$

The a_{Zr} is the same in all phases. For the Ru phase:

$$a_{Zr}^{Ru} = \gamma_{Zr}^{Ru} \, x_{Zr}^{Ru} = 10^{-5.191}$$

From the microprobe analysis of the C-Zr-Ru samples:

$$x_{Zr}^{Ru} = 0.0075 = 10^{-2.125}$$

Therefore:

$$\gamma_{Zr}^{Ru} = a_{Zr}^{Ru} / x_{Zr}^{Ru} = 10^{-5.191} / 10^{-2.125}$$

$$\gamma_{Zr}^{Ru} \text{ (0.75 at.\% Zr)} = 10^{-3.067}$$

It is sometimes convenient to know the activity coefficient of an element at the limit of 0% of that element in an alloy. Using solution theory one can calculate the activity coefficient of Zr in Ru in the limit of 0% Zr. An equation describing the variation of a_{Zr} as a function of composition can be expressed as:

$$2.303 \, RT \log_{10} \gamma_{Zr}^{Ru} = \alpha x_i^2 + b \qquad (2)$$

where $\alpha = V_{Zr}[(\Delta E/V)_{Zr}^{1/2} + (\Delta E/V)_i^{1/2}]^2$ which is the regular solution contribution to γ_{Zr}. The V_{Zr} and V_i are the respective molar volumes of Zr and the other element in solution; ΔE_{Zr} and ΔE_i are the respective energies of vaporization. The α accounts for differences in internal pressure

between the elements. The "b" term is the sum of all other contributions to the γ_{Zr} and is a function of composition. Equation (2) will be applied to the Zr systems of Ru, Ir and Au. For these systems the largest interaction is the sharing of electron pairs with Zr and it will be the dominant parameter in the "b" term. It represents the change of γ_{Zr} associated with charge transfer. Leo Brewer's predictions[3] indicate that Zr will change from a $(d^2s'p')$ configuration to a configuration that will more closely match the electronic configuration of the solvent element in the lattice. The "b" term will be large but it will be constant over the range of low concentrations of Zr to be discussed. The "α" term for the Zr-Ru system can be evaluated knowing the appropriate internal pressure parameters, also referred to as solubility parameters; Leo Brewer lists the values for the elements in Table XXIII[3]:

$$[(\Delta E/V)_{Zr}]^{1/2} = 102 \text{ cal}^{1/2}/\text{cc}^{1/2}$$

$$[(\Delta E/V)_{Ru}]^{1/2} = 135 \text{ cal}^{1/2}/\text{cc}^{1/2}$$

These values are for neutral Zr and Ru. Using the Engel Correlation and the Brewer Predictions, the electronic configuration expected for the hcp Ru phase is $(4d^{6.3}5s^{1.0}5p^{0.7})$ which has 3.7 d electron bonds per atom. If the Zr is to take full advantage of the Ru bonding, it would have a configuration of $(4d^{3.7}5s^{1.0}5p^{0.7})$ and a corresponding formal charge of -1.4. One would predict, therefore, an internal pressure and volume similar to Nb and Mo:

$$[(\Delta E/V)_{Zr\ -1/4}]^{1/2} = \left\{[(\Delta E/V)_{Nb}]^{1/2} + [(\Delta E/V)_{Mo}]^{1/2}\right\}/2 = 128 \text{ cal}^{1/2}/\text{cc}^{1/2}$$

$$V_{Zr\ -1/4} \cong (V_{Nb} + V_{Mo})/2 = 10.2 \text{ cc.}$$

Therefore,

$$\alpha_{Zr\text{-}Ru} = 10.2\ [128 - 135]^2 \text{ cal}$$
$$= 499.8 \text{ cal}$$

Using this value in Eq. (2), the γ_{Zr}^{Ru} (0% Zr) can be calculated:

$$\log_{10} \gamma_{Zr}^{Ru} \text{ (0\% Zr)} - \log_{10} \gamma_{Zr}^{Ru} \text{ (0.75 at.\% Zr)} =$$
$$\frac{(499.8)\ [1-(0.9925)^2]}{(4.575)\ (1773^\circ K)} = 9.21 \times 10^{-4}$$

The "b"'s cancel, therefore:

$$\log_{10} \gamma_{Zr}^{Ru} \text{ (0\% Zr)} = -3.067 + 9.21 \times 10^{-4}$$
$$= -3.066$$

Ternary systems similar to the C-Zr-Ir system are somewhat different. The activity of Zr is calculated as above:

$$a_{Zr}^{ZrC} = 10^{-5.191}$$

In this system the $ZrIr_3$ phase is in equilibrium with ZrC and C. Therefore:

$$x_{Zr}^{ZrIr_3} = 0.25 = 10^{-0.602}$$

and

$$\gamma_{Zr}^{ZrIr_3} \text{ (25 at.\% Zr)} = 10^{-5.191}/10^{-0.602}$$
$$= 10^{-4.589}$$

The γ_{Zr}^{Ir} (0% Zr) cannot be calculated as before, however. Although the concentration range of $ZrIr_3$ is very narrow, the a_{Zr} may change rapidly with composition. The range of the $a_{Zr}^{ZrIr_3}$ is not known even though one point within the range has been determined. As a result one can only say that $a_{Zr}^{ZrIr_3} = 10^{-5.191}$ is greater than the a_{Zr} at the Ir-rich side of the $ZrIr_3$ phase. Since a_{Zr} at the Ir-rich phase boundary of $ZrIr_3$ is equal to that of Zr in the Ir phase, this activity of Zr can be expressed as

$a_{Zr}^{ZrIr_3\text{-}Ir}$ and : $a_{Zr}^{ZrIr_3\text{-}Ir} \leq 10^{-5.191}$ at 1500°C.

In order to determine the γ_{Zr}^{Ir} (0 at.% Zr) several estimates must still be made. Leo Brewer[3] has predicted the solubility of Zr in the Ir phase to be 15 at.% at the eutectic temperature. Although the eutectic temperature is probably around 2000°C, neither the eutectic temperature nor the solubility of Zr in Ir have been experimentally determined. Assuming a solubility of Zr in Ir at the eutectic temperature, the solubility of Zr in Ir at 1500°C would have to be calculated. This calculation would depend upon the entropy difference of Zr in the $ZrIr_3$ phase and in the Ir phase over the Zr concentration range of 15 to 0 at.%. The entropy difference would depend upon the differences in the ordering in the internal pressure, in the Coulombic interactions, and in the charge transfer between the two phases. All of the above would raise the a_{Zr}^{Ir} $(0.15 \leq x_{Zr} < 0)$ relative to $a_{Zr}^{ZrIr_3}$ except the last factor which would lower the value. Once the x_{Zr}^{Ir} at the Ir-rich boundary was known at 1500°C, the upper limit on the γ_{Zr}^{Ir} could be calculated because of a_{Zr} at this point is known : $a_{Zr}^{ZrIr_3\text{-}Ir} \leq 10^{-5.191}$. The γ_{Zr}^{Ir} (0 at.% Zr) could then be calculated if $\gamma_{Zr}^{Ir} = f(x_{Zr}^{Ir})$ were known; the solution theory discussed for the Zr-Ru system also holds for the Zr-Ir system. Within the accuracy of these many assumptions:

$$\gamma_{Zr}^{Ir} \text{ (0\% Zr)} \simeq \gamma_{Zr}^{ZrIr_3\text{-}Ir} \leq 10^{-4.59}$$

B. The Gibbs Free Energy of Formation from Ternary Phase Diagrams

From ternary phase diagrams such as those of Figs. 1 and 2, information can be obtained on the Gibbs free energy of formation (ΔF_f) of all the intermetallic binary Zr compounds represented in the ternary diagrams.

Considering the C-Zr-Ir system first, the following reaction may be written because ZrC and Ir cannot exist in equilibrium according to the ternary phase diagram presented in Fig.1.

$$ZrC + 3Ir \rightarrow ZrIr_3 + C$$

This reaction was actually observed at 1500°C; the details of the reaction will be discussed later. Since the reactants and the products are solids, the free energy of the reaction (ΔF_{rx}) may be expressed by the approximate relation:

$$\Delta F_{rx,T} = \Delta H_{rx,\ 298} - T\Delta S_{rx,\ 298}$$

and $\Delta S_{rx,\ 298}$ may be assumed zero. Thus the free energy of the reaction is rather insensitive to temperature and if $\Delta F_{rx,T}$ is found to be less than zero, $\Delta F_{rx,298}$ may also be assumed to be less than zero. At 298°K ΔF°_f (ZrC) = -46.2 ± 0.3 kcal/mole ,[10] and ΔF°_f of all elements is zero. A limit on ΔF°_f ($ZrIr_3$) can be obtained. Since the reaction occurred:

$$\Delta F^\circ_{rx,298} \leq 0$$

Therefore:
$$\Delta F^\circ_{rx} = \Delta F^\circ_f (ZrIr_3) - \Delta F^\circ_f(ZrC) \leq 0$$

$$\Delta F^\circ_f (ZrIr_3) \leq \Delta F^\circ_f (ZrC) = -46.2 \text{ kcal/mole at } 298°K$$

Thus, the limit obtained is $\Delta F^\circ_f(ZrIr_3) \leq -46.2$ kcal/mole or -11.5 kcal/gram atom as listed in Table VI.

With a knowledge of what Zr-Ir compounds are thermodynamically stable with respect to each other, more limits may be determined. The following inequality is true for such compounds in the Zr-Ir system:

$$1/3\ \Delta F^\circ_f (Zr_3Ir) \geq 1/2\ \Delta F^\circ_f (Zr_2Ir) \geq 3/5\ \Delta F^\circ_f (Zr_{5/3}Ir) \geq \Delta F^\circ_f (ZrIr) \geq \Delta F^\circ_f (ZrIr_2) \geq \Delta F^\circ_f (ZrIr_3) \quad (1)$$

The above can be rationalized by considering reactions such as:

$$ZrIr_2 + Ir \rightarrow ZrIr_3 \quad \text{and}$$

$$1/3\ Zr_3Ir + 1/6\ Ir \rightarrow 1/2\ Zr_2Ir$$

$\Delta F^\circ_{rx} \leq 0$ for both reactions because these Zr-Ir compounds are reported as stable with respect to each other. Another similar inequality is true:

$$\Delta F^\circ_f (Zr_3Ir) \leq \Delta F^\circ_f (Zr_2Ir) \leq \Delta F^\circ_f (Zr_{5/3}Ir) \leq \Delta F^\circ_f (ZrIr) \leq 1/2\ \Delta F^\circ_f (ZrIr_2) \leq 1/3\ \Delta F^\circ_f (ZrIr_3) \qquad (2)$$

which can be rationalized by considering reactions such as:

$$Zr_2Ir + Zr \rightarrow Zr_3Ir \quad \text{and}$$

$$1/3\ ZrIr_3 + 1/6\ Zr \rightarrow 1/2\ ZrIr_2$$

where $\Delta F^\circ_{rx} \leq 0$. The ΔF°_f's expressed in inequalities (1) and (2) have units of kcal/mole; the ΔF°_f's in Table VI are expressed in kcal/gram atom. These same inequalities can be derived by considering free energy diagrams as presented by L. S. Darken and R. W. Gurry.[19] Using inequality (2) along with the inequality $\Delta F^\circ_f (ZrIr_3) \leq -46.2$ kcal/mole, the limits of Table VI can be obtained. Inequality (1) would be used if there were any compounds to the Ir rich side of $ZrIr_3$.

The ternary systems represented in Fig. 2 are different. For Ru alloys it has experimentally been determined at 1500°C that Ru (0.75 at. % Zr) exists in equilibrium with the C and the ZrC phases and that the $ZrRu_2$ and the Ru (1.15 at.%Zr) binary phases exist in equilibrium without the presence of both C and ZrC. The experimental details used to obtain

these conclusions will be covered later. From this information the $\Delta F^{\circ}_{f}(ZrRu_2)$ can be estimated and limits can be placed on the Gibbs free energy of formation of ZrRu, the only other known Zr-Ru binary alloy.

From the three phase equilibrium of C, ZrC, and Ru (0.75 at.% Zr) at 1500°C (1773°K):

$$a_{Zr} = 10^{-5.191}$$

as calculated previously.

$$\gamma^{Ru}_{Zr} \text{ (0.75 at.\% Zr)} = 10^{-5.191}/0.0075 = 10^{-5.191}/10^{-2.125} = 10^{-3.067}$$

Solution theory can be used to obtain γ^{Ru}_{Zr} (1.15 at.% Zr.) The internal pressure parameter for the Ru-rich side of the Zr-Ru binary system has been previously evaluated : α = 499.8 cal. Using Eq. (2):

$$\log_{10} \gamma^{Ru}_{Zr} \text{ (1.15 at.\% Zr)} = \log_{10} \gamma^{Ru}_{Zr} \text{ (0.75 at.\% Zr)} + \frac{(499.8\ (0.9885^2 - 0.9925^2))}{(4.575)\ (1773^{\circ}K)}$$

$$= -3.067 + 4.92 \times 10^{-4}$$

$$= -3.067$$

Therefore

$$\gamma^{Ru}_{Zr} \text{ (1.15 at.\% Zr)} = \gamma^{Ru}_{Zr}\, x^{Ru}_{Zr}$$

$$= (10^{-3.067})\ (10^{-1.939})$$

$$= 10^{-5.006}$$

The activity of Ru this close to pure Ru can be approximated by considering the Ru phase an ideal solution:

$$\gamma^{Ru}_{Ru} = 1$$

$$a^{Ru}_{Ru} \text{ (1.15 at.\% Zr)} = x^{Ru}_{Ru} = 0.9885 = 10^{-0.0050}$$

As stated above Ru(1.15 at.% Zr) exists in equilibrium with the $ZrRu_2$ phase. Therefore, from thermodynamics:

$$a_{Zr}^{Ru} \quad (1.15 \text{ at.\% Zr}) \quad = \quad a_{Zr}^{ZrRu_2}$$

and

$$a_{Ru}^{Ru} \quad (1.15 \text{ at.\% Zr}) \quad = \quad a_{Ru}^{ZrRu_2}$$

The standard state ΔF_f ($ZrRu_2$) may be expressed as ΔF_f° ($ZrRu_2$) = +RT ln a_{Zr} a_{Ru}^2. Knowing the appropriate activities, the ΔF_f° ($ZrRu_2$) can be calculated: ΔF_f° ($ZrRu_2$) = 2.303 RT $\log_{10}$ a_{Zr} a_{Ru}^2

= 4.575 (1773°K) (-5.006 - 2 × 0.0050)

= -40.69 kcal/mole at 1500°C

= -13.56 kcal/g.atom.

The above value is based on the various experimentally determined concentrations of Zr. From the microprobe analysis of a $Zr_{0.6}$ $Ru_{99.4}$ test standard, the Zr concentrations are in error by less than ±37% of the amount present; the corresponding error associated with the calculated ΔF_f° ($ZrRu_2$) is ±2.7 kcal/mole or ±0.9 kcal/g-atom. In the calculations it was assumed that log γ_{Zr}^{Ru} varies as $(x_{Ru}^{Ru})^2$ between 0.75 and 1.15 at.% Zr and that γ_{Ru}^{Ru} = 1 from 0 to 1.15 at.% Zr.

Inequality (1) gives: ΔF_f° (ZrRu) $\geq$ ΔF_f° ($ZrRu_2$); and inequality (2) gives: ΔF_f° (ZrRu) $\leq$ 1/2 ΔF_f° ($ZrRu_2$). Using these inequalities with the calculated ΔF_f° ($ZrRu_2$) and the estimated error, the following limits on ΔF_f° (ZrRu) are obtained:

$$-19.0 \text{ Kcal/mole} \geq \Delta F_f^\circ \text{ (ZrRu)} \geq -43.4 \text{ Kcal/mole}$$

Table VI gives these limits expressed in kilocalories/gram atom at 1500°C.

A similar procedure can be followed for the Zr-Au alloys. The calculation is more involved because the equilibration of C, ZrC, and Au (9.5 at.% Zr) was done above the melting points of Au and $ZrAu_4$ and the ΔF_f°'s are desired for solid alloys. The calculation is given in Appendix B. The calculated limits for ΔF_f°($ArAu_4$) are:

$$-37.9 \text{ kcal/mole} \geq \Delta F_f^\circ (ZrAu_4) \geq 41.4 \text{ kcal/mole at } 1000^\circ C$$

Although the C-Zr-Os and C-Zr-Ag phase diagrams are also of the type represented in Fig. 2, the method of estimating the ΔF_f°'s of these compounds represents still another case. The information necessary to calculate the ΔF_f°'s of the Os and the Ag rich binary alloys of Zr in a manner similar to the C-Zr-Ru system is lacking. The solubilities of Zr in the Os and the Ag phases in equilibrium with C and ZrC are not known; only solubility limits were obtained. For these systems limits on the ΔF_f°'s of the various binary compounds can be obtained in a fashion similar to that of the C-Zr-Ir system first discussed. Such systems have inequalities like (1) and (2); but ZrC is more stable than all the binary compounds. The appropriate limits can best be visualized by considering the reactions such as:

$$ZrOs_2 + C \rightarrow ZrC + 2Os.$$

Since ZrC and Os exist in equilibrium (as presented in Fig. 2), ΔF_{rx}° is less than zero. ΔF_{rx}° can be expressed as:

$$\Delta F_{rx}^\circ = \Delta F_f^\circ (ZrC) - \Delta F_f^\circ (ZrOs_2) \leq 0$$

which gives

$$\Delta F_f^\circ (ZrOs_2) \geq \Delta F_f^\circ (ZrC)$$

and at 298°K:

$$\Delta F_f^\circ (ZrOs_2) \geq -46.2 \text{ kcal/mole or } -15.4 \text{ kcal/g.atom}$$

which is listed in Table VI. In order to obtain limits on other compounds of the binary system, direct reaction with ZrC can be considered or inequality (1) can be used.

IV. DETERMINATION OF TERNARY PHASE DIAGRAMS

The general methods of sample preparation, analysis, and data computation have been discussed. Some individual aspects of the various systems bear comment.

A. The C-Zr-Rh, C-Zr-Ir, C-Zr-Pd, and C-Zr-Pt Systems

The C-Zr-Ir system was the first to be investigated. One mole of ZrC and three moles of Ir powder were mixed and hot pressed for 15 minutes at 1585°C and 500 atmospheres pressure. X-ray analysis showed a 50% conversion to $ZrIr_3$. Three additional hours showed almost complete reaction and three more hours showed no further change. Although the two phases of $ZrIr_3$ and C were probably not in final equilibrium within three hours, the equilibrium phases had already been formed. Analysis of the ZrRu + 1.2C reaction also verified that a three hour reaction time was sufficient to observe the products which would exist in equilibrium eventually. A three hour reaction time was, therefore, chosen for the reactions when only the equilibrium phases were to be determined; longer times were used when the concentrations of the equilibrium phases were desired, as in the C-Zr-Ru system.

Since the ZrM_3 ordered structure is present in the Zr binary systems of Rh, Pd, and Pt as well, similar reactions were run and the two phase equilibrium between C and the ZrM_3 structure was observed in all cases. J. M. Criscione et al. observed similar reactions for ZrC with Rh and Ir between 1200°C and 2200°C.[20]

To pin down the three phase regions of the diagrams, samples were made with a surplus of ZrC. The details of the reactions are given in Table II. The Ir phase listed under "Phase Observed" had low intensity peaks after heating and is considered to be unreacted material. The graphite peak at d = 3.3334Å was observed in the Rh and Pt systems; although not observed by x-ray diffraction in the C-Zr-Ir and C-Zr-Pd systems, it was observed by metallographic examination.

The reactions given in Table II are not balanced. If they were, the reactions would be $ZrC + 3M \rightarrow ZrM_3 + C$. The format of Table II was chosen to show the equilibrium phases actually observed.

Figure 1 represents the type of ternary diagram determined; the solid joins indicate that ZrM_3 was experimentally observed to be in equilibrium with ZrC and C. Although the dashed joins are drawn for the C-Zr-Ir system, they indicate that Zr alloys of Rh, Pd and Pt as well as Ir to the Zr-rich side of the ZrM_3 phase exist in equilibrium with ZrC. Those compounds to the M rich side of the ZrM_3 phase exist in equilibrium with graphite. The above assumes no ternary compound formation.

Thermodynamic data on the Zr binary systems were obtained in the straightforward manner outlined in Part III. The resulting $\bar{F}_{Zr}^{xs}$ and ΔF_f° information is given in Tables V and VI respectively.

Some information was gained on the liquidus phase of the ternary diagrams. A ZrC + 3 Ir sample heated to 2000°C melted indicating that the liquidus phase appears below 2000°C but above the 1575°C reaction temperature. J. M. Criscione et al.[20] observed the melting of a ZrC + 3Ir sample at 2100°C, essentially in agreement with the above. None of the other samples showed signs of melting at the reaction

temperatures listed in Table II. A ZrC + 3Rh sample prepared by J. M Criscione et al. was heated to 2200°C; it did not melt.

B. Miscellaneous Properties of $ZrIr_3$ and $ZrPt_3$

A separate sample of $ZrIr_3$ was made from the elements and was heated on a tungsten plate in a vacuum furnace. Its observed melting points is 2126±133°C.

An attempt was made to etch the pure $ZrIr_3$ sample. Among the stronger treatments were: boiling in aqua regia for 1-1/2 hours; boiling in concentrated HF for 1-1/2 hours; boiling in a solution of aqua regia and concentrated HF for 1/2 hours; heating in molten KOH for 1-1/2 hours. All of these chemical reagents left the sample's shiny metallographically polished surface unattacked. Heating the sample in an air furnace at 1000°C for 1/2 hour caused the surface to ripple slightly as if the sample were being annealed. The polished surface still was shiny; no oxide buildup was visible.

$ZrIr_3$ was not found to be superconducting between 1.4 and 18°K. $ZrIr_3$ is brittle and it is easily ground.

George Stowe[21] determined the ΔF_f° ($ZrPt_3$) at 1000°C to be less than -80 kcal/mole by observing the reaction $ZrO_2 + 3\ Pt + 2\ H_2(g) \rightarrow ZrPt_3 + 2H_2O(g)$. ZrO_2 and Pt powders were mixed in the ZrO_2:Pt molar ratios of 1:2, 2:3, and 4:5 and pressed into pellets 1/2" × 3/16". A ZrO_2 blank was also made. Each sample was placed on platinum foil in a nickel boat and was heated in a tube furnace. H_2 gas was passed through the furnace for periods of 14 to 17 hours. Furnace runs were made at 800°C, 1000°C, and 1150°C. In each case the sample was furnace cooled using a flow of 4% H_2/He atmosphere. X-ray diffraction patterns of the pellet surfaces identified the $ZrPt_3$ (hcp) in the $4ZrO_2 + 5$ Pt heatings at 1000°C and at 1150°C and in the $ZrO_2 + 2Pt$ and $2ZrO_2 + 3Pt$ heatings at 1150°C.

The sample weight loss was used to calculate the moles of $H_2O(g)$ formed. The weight loss of the ZrO_2 blank heated in H_2 at these temperatures was subtracted to correct for adsorbed water. The flow of H_2 was monitored and the total amount used was on the order of 6 moles. The above calculation gave a ratio equal to the pressure ratio of H_2O to H_2 which is less than the equilibrium value of P_{H_2O}/P_{H_2}. From this information limits on ΔF_f° ($ZrPt_3$) were obtained:

$$\Delta F_f^\circ(ZrPt_3) \leq -80 \text{ kcal/mole at } 1000^\circ C \text{ and } \Delta F_f^\circ (ZrPt_3) \leq -76 \text{ kcal/mole at } 1150^\circ C.$$

A sample calculation follows: at 1000°C, the $4ZrO_2 + 5Pt$ sample lost 0.045 grams, after correcting for the ZrO_2 blank weight loss. Dividing by the molecular weight of oxygen (O) indicates that 2.815 ± 10^{-3} moles of H_2O were formed. Dividing by the moles of H_2 passed through the furnace (6 moles) indicates that $(P_{H_2O}/P_{H_2}) = 4.69 \pm 10^{-4}$. Since equilibrium was not reached:

$$\left(\frac{P_{H_2O}}{P_{H_2}}\right)_{equilibrium} \geq \left(\frac{P_{H_2O}}{P_{H_2}}\right)_{measured}$$

and

$$-RT \ln \left(\frac{P_{H_2O}}{P_{H_2}}\right)^2_{equilibrium} \leq -Rt \ln \left(\frac{P_{H_2O}}{P_{H_2}}\right)^2_{measured} \leq +39 \text{ kcal.}$$

For the reaction:

$$ZrO_2 + 3Pt + 2H_2(g) \rightarrow ZrPt_3 + 2H_2O(g)$$

at equilibrium:

$$\Delta F_f^\circ = -RT \ln (P_{H_2O}/P_{H_2})^2_{equilibrium}$$

ΔF_{rx}° can be calculated from the free energy function and ΔH_{298}° tables[67] as:

$$\Delta F^\circ_{rx} = \Delta F^\circ_f (ZrPt_3) + 119 \text{ kcal.}$$

From the above:

$$\Delta F^\circ_f(ZrPt_3) = -119 \text{ kcal} - 2 RT \ln \left(P_{H_2O}/P_{H_2}\right)_{equilibrium}$$

$$\leq -119 \text{ kcal} - 2 RT \ln \left(P_{H_2O}/P_{H_2}\right)_{measured}$$

$$\leq -119 + 39 \text{ kcal}$$

$$\Delta F^\circ_f(ZrPt_3) \leq -80 \text{ kcal at } 1000^\circ C$$

Assuming that the entropy of formation (ΔS°_f) and ΔC°_p of formation are zero, ΔF°_f ($ZrPt_3$) at 1000°C = ΔH°_f ($ZrPt_3$) at 1000°C = $\Delta F^\circ_f(ZrPt_3)$ at 298°K = ΔH°_f ($ZrPt_3$) at 298°K. Therefore, ΔH°_f ($ZrPt_3$) $\leq$ -80 kcal/mole.

A student of Wayne L. Worrell has run some preliminary EMF measurements on $ZrPt_3$. Initial experiments indicate that ΔF°_f ($ZrPt_3$) is in the vicinity of -80 kcal/mole.[22]

C. The C-Zr-Ru and C-Zr-Os Systems

One mole of ZrC, seven moles of Ru, and an unmeasured amount of graphite were hot pressed for seven hours at 1500°C and 200 bars pressure. X-ray diffraction showed no phase change. Microprobe analysis indicated that 0.20 at.% Zr had dissolved into the Ru phase. The sample was heated for an additional 123 hours which brought the concentration to 0.74 at.% Zr. To make sure that there was no kinetic barrier, a ZrRu alloy was made to be reacted with graphite. The elemental powders were mixed, cold pressed, arc melted, and homogenized for one hour at 2020°C. Microprobe analysis indicated that the sample was homogeneous. The ZrRu sample was easily ground to < 200 mesh. Graphite was added to make a molar ratio of ZrRu to C of 1.0 to 1.2. After 3 hours of hot pressing at 1500°C, the reactants were x-rayed and ZrC, $ZrRu_2$, and Ru were found to be present indicating that the reaction was not complete. After a total of 7 hours, no $ZrRu_2$ remained but the Ru phase grain size was too small to microprobe for the at.% Zr. Annealing the sample 81 additional hours did promote grain growth. Microprobe analysis indicated that 0.76 at.% Zr was present in the Ru phase.

The summary of the reactions is presented in Table III. They indicate that at 1500°C, Ru with 0.75 at.% Zr is in equilibrium with C and ZrC. Using Eq. (1), γ_{Zr}^{Ru} (0.75 at.% Zr) = $10^{-3.067}$. The other desired thermodynamic information is derived in Part III.

A sample of Ru (0.6 at.% Zr) was made in order to check the microprobe accuracy; however, small inclusions of high Zr content could not be homogenized into the Ru phase, not even after 146 hours at 1540°C. The Ru phase analyzed as 0.38 at.% Zr; therefore, the at.% Zr reading is at least within ±37% of the actual value. No correction factor is

added to the microprobe results because of the difficulty in getting a good microprobe standard.

Some of the samples gave information on the liquidus phase in the ternary system. A sample of ZrC + 7Ru + 3.2C heated in a graphite crucible to 1870°C had melted while the ZrC + Ru + C samples heated to 1500°C did not melt. A Zr_7Ru_{93} alloy consisting of the Ru and the $ZrRu_2$ phases fused to a ZrC crucible at 1700°C; the liquid phase was not encountered when the Zr_7Ru_{93} sample was heated in a ZrC crucible to 1520°C for 141 hours.

The C-Zr-Os system was expected to be analogous to the C-Zr-Ru system. A $ZrOs_2$ alloy was made from the elemental powders and hot pressed with graphite in a mole ratio of 1.0:1.1::$ZrOs_2$:C. After 12 hours at 175 bars pressure and 2 hours at 350 bars all at 1480°C in Ar, x-ray analysis showed that the reaction was complete with C, ZrC, and Os being the product phases. The Os grains were too small to obtain unambiguous at.% Zr microprobe readings without interference from the ZrC phase. An additional heating in the vacuum furnace brought the total time at 1490°C to 154 hours. The Os phase was still difficult to microprobe because of interference from the ZrC phase. Accepting only the lowest readings obtained from the sample gave 0.24 at.% Zr in the Os phase.

In both the ZrRu + 1.2C sample and the $ZrOs_2$ + 1.1 C sample, the elemental grain size posed a problem. Although the microprobe's concentrated beam is 1 to 2 microns in diameter, its fringe area must be larger, possibly 5 to 10 microns in diameter. As a result, a small inclusion of 2 micron diameter can be detected but not quantitatively analyzed.

Also, small inclusions of a second phase can interfere with the quantitative analysis of a large phase. The C-Zr-Ru and C-Zr-Os equilibrations are fine examples of this difficulty. The Zr counts of the ZrC phase were on the order of 20,000 counts/20 sec, and those of the Ru phase were 40 counts/20 sec; a very small quantity of ZrC can interfere markedly with the Zr counts off of the elemental phase. Figures 4 and 5 are pictures of the metal surfaces at 400×, the power of the microscope on the MAC microprobe. When C, ZrC, and Ru were the reactants, Fig. 4(a), the phases were large because there was no phase change and because the reactant powders were large relative to the microprobe beam size. With ZrRu and $ZrOs_2$ as initial phases, Figs. 4(b) and 5(b), the ZrC, Ru, and Os phases had to nucleate and grow; therefore, their size is much smaller and the ZrC phase is dispersed throughout. The 2 micron stepping mechanism for diffusion analysis was employed to transverse seemingly clean elemental phases. The mechanism automatically moves the sample 2 microns, stops to read the count, and repeats the process continuing in a straight line. Only the lowest Zr readings were used to determine the at.% Zr present. In both Figs. 4(b) and 5(b) small inclusions of ZrC can be seen in the elemental phases.

The ZrRu + 1.2C sample agrees well with the other C-Zr-Ru sample. In order to avoid any ambiguity in the C-Zr-Os system, a sample of ZrC + 7Os + xC (an unmeasured amount of graphite) was made from powder, mixed, and hot-pressed at 1870°C for 17-1/4 hours. Microprobe analysis indicated that 0.62 at.% Zr had dissolved into the Os phase. Heating the sample for 120 hours at 1495°C left such a low level of Zr in the Ox phase that it could not be detected by the electron microprove. In both cases the microprobe analysis of the sample was straightforward; the grain size of the

Os was large with no small inclusions of ZrC. Figure 5(a) shows the sample after the five day heating at 1495°C. The elemental phases in Figs. 4 and 5 appear as white and the ZrC phase appears as gray. The black areas represent pull out of chunks of the sample due to the interlacing of the relatively weak graphite phase and due to porosity.

In order to determine the detection limit of the microprobe, the formula presented by H. S. de Ben[17] is used:

$$C_{DL} = \frac{1.47\sqrt{\bar{N}_b}}{\bar{N}_s - \bar{N}_b} C_s \qquad (3)$$

where C_{DL} ≡ concentration at the limit of detection of the microprobe (80% confidence); N_b ≡ average background counts per unit time. C_s ≡ concentration of the standard used. It has been stated that Eq. (3) cannot be used to assign an error limit to the microprobe readings; that is, if the microprobe analysis of a sample gives a concentration of an element equal to C_{DL} calculated from Eq. (3), then the analysis cannot be assigned a confidence limit of 80% automatically. The equation can be used, however, to determine the detection limit of the microprobe since the Zr background counts from the pure Os standard were identical to the Zr counts from the Os phase of the sample. Using the appropriate values for the C + ZrC + Os sample is Eq. (3):

$$C_{DL} = \left[1.47\sqrt{34}/\,30(492-34)\right]100\%$$
$$= 0.028 \text{ wt.\% Zr.}$$
$$= 0.059 \text{ at.\% Zr}$$

The above reactions show that when the C, ZrC and Os phases exist in equilibrium at 1500°C, the concentration of Zr in the Os phase is

less than 0.06 at.% Zr. Using Eq. (1), γ_{Zr}^{Os} ($\leq$ 0.06 at.% Zr) $\geq 10^{-1.96}$. The other thermodynamic data are presented in Tables V and VI.

Information on the liquidus phase was gained when a $ZrOs_2$ sample was heated in a ZrC crucible to 2480°C. It melted at the point of contact with the crucible. A sample heated to 2020°C did not melt.

D. The Zr-Ru and Zr-Os Binary Systems

A sample of $Zr_{7.5}Ru_{92.5}$ was made from elemental powders and annealed for 141 hours at 1520 ± 80°C. It took three to five minutes for the red glow of the furnace to disappear, i.e. to reach ~ 750°C. Metallographic analysis showed two phases were present; x-ray diffraction identified them as Ru and $ZrRu_2$. Electron microprobe analysis indicated that 1.15 at.% Zr in the Ru phase exists in equilibrium with the $ZrRu_2$ phase at 1520 ± 80°C.

A $Zr_{1.4}Os_{98.6}$ alloy was arc melted and was homogenized for 13-1/2 hours at 1525 ± 65°C. Metallographic analysis indicated that two phases existed. The large Os phase was analyzed with the microprobe and found to have a Zr concentration less than the detection limit of the microprobe, $\leq$ 0.06 at.% Zr.

The melting points of ZrRu and $ZrOs_2$ were experimentally determined to be 2130 ± 70°C and 2573 ± 80°C, respectively. Both compounds are brittle and exhibit no superconductive or ferromagnetic transformation between 1.4 and 18°K.

E. The C-Zr-Ag and C-Zr-Au Systems

As indicated in Table IV, the solid state reactions of the C-Zr-Ag and C-Zr-Au systems did not proceed; x-ray diffraction patterns for the reactants and the products were the same.

Silver sponge and ZrC and graphite powders were heated in the induction furnace for 15 hrs at 1410°C. The silver formed a pool on top of the powder and did not mix well with the ZrC and C. Microprobe analysis of the Ag phase indicated that the Zr concentration was below the detection level of the microprobe. To check the kinetics of the reaction, the ZrAg + 1.2C sample which had been hot-pressed in the solid form was heated in the induction furnace for 10 hours at 1500°C. Inspection indicated that liquid Ag with some Zr content had flowed from the pressed pellet and attacked the graphite crucible. Metallographic analysis showed that a thin layer of ZrC existed between the graphite crucible and the Ag pool. Microprobe analysis verified the existence of the ZrC phase. Readings taken from the Ag both near the ZrC phase and into the interior of the phase showed that the Ag phase was homogeneous and that the Zr concentration was below the detection level of the microprobe. Referring to H. S. de Ben's work[17] again:

$$C_{DL} = \frac{1.47\sqrt{\bar{N}_b}}{\bar{N}_s - \bar{N}_b} \qquad (3)$$

$$= \frac{1.47\sqrt{11}}{11581-11}$$

$$= 0.042 \text{ wt.\% Zr}$$

$$= 0.050 \text{ at.\% Zr}$$

When liquid Ag is in equilibrium with ZrC and C at 1500°C, the concentration

of Zr in the Ag phase is less than 0.05 at.% Zr.

Au sheet, ZrC powder and C powder making a stoichiometric ratio of 3.0:1.1:0.1 respectively were heated in the induction furnace at 1495°C for 12-1/4 hours. The liquid Au formed a bead on top of the ZrC and C powder as if it did not wet the powder. Microprobe analysis indicated that 0.87 at.% Zr had dissolved into the Au phase. Gray areas giving a lower count of Zr than on the Au phase appeared as two phases, C and Au, when examined under the microscope. Such a formation indicates that some C did dissolve in the Au at 1500°C but it precipitated out on cooling. The Au phase did appear to be homogeneous with respect to Zr concentration.

Some of the $Zr_{3.40}Au_{96.60}$ alloy previously used as a test standard was heated with ZrC and C in the induction furnace for 12-1/3 hours at 1505°C. No change in the composition of the alloy was observed by microprobe analysis. As a result, no thermodynamic data were derived from this observation.

A sample of $ZrAu_3 + ZrAu_4 + C$ which had been hot-pressed but had not reacted was heated inductively for approximately 30 hours. The sample did not appear to have reacted. It was a black powder as it was before the heating; no liquid Au phase was visible. In the powder form, the sample could not be mounted for electron microprobe analysis. X-ray diffraction of the powder indicated that a reaction had occurred; the Au, ZrC and C phases were observed. No $ZrAu_4$ phase was evident.

In order to obtain a Au phase large enough to be analyzed with the microprobe, a $ZrAu_3 + ZrAu_4 + C$ sample was heated in the hot press for 111-1/2 hours at 1515°C±65°C with no applied pressure. The sample was then hot pressed at 350 bars pressure for 1/2 hour and cooled. The

liquid Au alloy which had squeezed out of the hot press was analyzed with the microprobe and found to contain a $ZrAu_4$ phase containing 20.5 ± 1.0 at.% Zr and a Au phase containing 7.0±1.0 at.% Zr. Metallographic analysis using standard area measuring techniques[23] indicated that 40.0±4.4 volume % of the sample was $ZrAu_4$. Using the theoretical molar volumes calculated from lattice constant information on Au[24] and $ZrAu_4$,[57] the volume percent was converted to the overall percent of Zr in the liquid phase at 1500°C: 12.1±1.2 at.% Zr. The details of this calculation are presented in Appendix B. One of the droplets had $ZrAu_4$ and Au phases so small that they could not be analyzed separately; the microprobe readings of the sample indicated the droplet contained 11 at.% Zr.

The four liquid C-Zr-Au samples discussed do not give a very narrow range of the concentration of Zr in liquid Au at 1500°C. Interpreting the data broadly, one can say that 8.5±7.0 at.% Zr in the Au phase exists in equilibrium with ZrC and C. The samples of pure Au and Au (3.40 at.% Zr) did not wet the ZrC and C powder reactants; the liquid formed a droplet on top of the powder. In the Zr rich sample, the Au alloy phase apparently did wet the ZrC and C powders because the one sample that could not be microprobed still remained as a black powder. In this sample, however, no $ZrAu_4$ could be detected by x-ray diffraction. The $ZrAu_4$ structure is a modified hcp structure and the peaks are lower than the fcc Au structure; however, 40 volume percent of $ZrAu_4$ relative to the Au phase should have been detected. From this sample, the equilibrium percent Zr in Au may be expected to be 7.0 at.% Zr.

By correlating all the experimental observations, the Zr concentration is most likely 7.0±1.0 or 12.1±1.2 at.% Zr. Averaging these two values, Au (9.5±3.5 at.% Zr) exists in equilibrium with C and ZrC at

1500°C can be calculated from Eq. (1):

$$\gamma_{Zr}^{Au} \text{ (6.0 at.\% Zr)} = 10^{-5.191}/10^{-1.222} = 10^{-3.969}$$

$$\gamma_{Zr}^{Au} \text{ (13.0 at.\% Zr)} = 10^{-5.191}/10^{-0.886} = 10^{-4.305}$$

Therefore:

$$10^{-3.97} \geq \gamma_{Zr}^{Au} \text{ (9.5±3.5 at.\% Zr)} \geq 10^{-4.317}$$

Using Eq. (2) and the appropriate values as given in Appendix B:

$$10^{-3.824} \geq \gamma_{Zr}^{Au} \text{ (0 \% Zr)} \geq 10^{-4.211} \text{ at 1500°C.}$$

The other thermodynamic data are found in Tables V and VI.

F. The C-Zr-Re System

Since the Ru and the Os phases exist in equilibrium with ZrC and C, it was expected that the Re phase might also exist in equilibrium with ZrC and C. The Zr_5Re_{24} phase is the most Re rich phase of the Zr-Re system; it was made to be reacted with C.

The Zr_5Re_{24} phase is reported to exist over a composition range of not more than 5 at.% Zr (3 wt.%).[26] A Re zone refined rod and Zr cold pressed powder were used to make an alloy of 16.6 at.% Zr as determined by accurate weighing of the original materials. Arc melting the sample was complicated by the fact that stresses were built up in the sample as it cooled after melting. After flipping the sample, initial heating with the arc made the sample fly apart. The Zr_5Re_{24} was annealed for 2 hours at 2000±70°C in a vacuum of 1×10^{-5} Torr. Six hundred Torr of He was added to the furnace at the end of the heating and the sample cooled to ~ 750°C in about eight minutes. Microprobe analysis indicated that the sample was homogeneous and that it contained

17.5 at.% Zr. The 5% error between the microprobe readings and the original weighing is within the expected accuracy.[13-15] The Zr_5Re_{24} alloy was used as a test standard for the microprobe readings of the Re phase of the ternary C-Zr-Re system. The microprobe values are multiplied by 0.95, equal to 16.6/17.5, as a correction factor but the ±5% error is retained as an expected accuracy.

A portion of the Zr_5Re_{24} compound was ground to less than 200 mesh and reacted with graphite in the respective molar ratio of 1 to 5.5. After 72 hours at 1500°C and 350 bars, x-ray analysis indicated that the Re phase was present, that the Zr_5Re_{24} phase had disappeared, and that the ZrC phase had not appeared. Microprobe analysis indicated that the Zr concentration had remained unchanged, however. Since the Re phase extends to about 2 at.% Zr[27] and does not extend to 16.6 at.% Zr in the binary phase, the resultant equilibrium Re phase must be ternary.

To determine the concentration of Zr in the Re phase in equilibrium with both ZrC and C, the reaction as given in Table III was run. Microprobe analysis indicated that the C and the ZrC phases exist in equilibrium with a Re phase containing a molar ratio of Zr to Re of 19.0 ± 1.0 to 81.0 ± 1.0. The % C is not known. Since the graphite has effected the binary alloys present, thermodynamic information of the binary Zr-Re system cannot be obtained from these empirical observations.

The lattice parameters of the hexagonal structure of the Re (Zr:Re: 19.0:81.0) alloy were determined to be a_o = 2.7810±0.0004Å, c_o = 4.4590 ±0.0008Å. The computer program used to refine the lattice parameters was written by Donald E. Williams, Ames Laboratory.[27] The phase observed may be a ternary alloy separate from the Re phase, but this is unlikely because the lattice parameters are so close to those of pure Re: a_o = 2.7600Å, c_o = 4.4580Å.[24] A possible ternary phase diagram is given

in Fig. 3. The arrows indicate that the percent C has not been determined and may be any value as long as the Zr:Re ratio is 19.0:81.0. The Re phase boundaries need not be straight lines even though they are indicated as such. Since a change in Zr concentration from a high value to a low value was not experimentally observed, it is possible that the Re phase extends to higher Zr concentration.

G. Discussion of Tables V and VI

Tables V and VI and Figs. 1 to 3 summarize the results of the experimental work.

The first column in Table V gives the at.% Zr in the various ZrM_3 and elemental phases actually observed in equilibrium with C and ZrC. The activity coefficient for Zr (γ_{Zr}) corresponding to the above at.% Zr is derived at that concentration using the relation: $a_{Zr} = \gamma_{Zr} x_{Zr}$, Eq. (1). The $\log_{10} \gamma_{Zr}$ is expressed in column 3. Regular solution theory and other estimates are used to calculate γ_{Zr} (0 % Zr) as it is expressed in the fourth column. The partial molar excess free energy of Zr ($\bar{F}^{xs}_{Zr}$) in the limit of 0 at.% Zr is expressed in the last column. It is related to γ_{Zr} by the relation: $\bar{F}^{xs}_{Zr} = 2.303\ RT \log_{10} \gamma_{Zr}$. Either $\log_{10} \gamma_{Zr}$ (0 % Zr) or $\bar{F}^{xs}_{Zr}$ (0 % Zr) can be used to show the change in the "stability" of Zr as a function of atomic number. The trend is irrespective of composition since the comparison is made in the limit of 0 % Zr; it is purely a comparison of "stability" as measured by $\bar{F}^{xs}_{Zr}$ or γ_{Zr} versus atomic number. Not enough information is available to show a meaningful plot of $\bar{F}^{xs}_{Zr}$ versus atomic number but it can be seen from Table V that a peak in the stability of Zr in the noble metals is reached near Rh and Ru in the Fifth Period of the Periodic Table and near Ir and Pt in the Sixth Period.

Table VI is a compilation of the phases now reported in the literature for which thermodynamic information was determined; no new phases were observed. The melting points of ZrRu, $ZrOs_2$, and $ZrIr_3$ were determined experimentally by this work. Other melting points are given where published. A discussion of the phases reported in Table VI follows.

Elliott[28] reports three intermetallic compounds in the Zr-Re binary system: Zr_2Re, $ZrRe_2$, and Zr_5Re_{24}. These phases as reported in Table VI are in agreement with E. M. Savitskii and M. A. Tylkina[26] except for Zr_5Re_{24} which may be a superlattice similar to Ti_5Re_{24}.

R. E. Wang in a recent paper[29] on ZrRu, ZrRh, and ZrPd found that ZrRh and ZrPd behave in a manner similar to TiNi with its "martensitic" transformation. ZrPd at room temperature (R.T.) was found to be analogous to TiNi at or below its M_f temperature. This TiNi structure has not been fully determined butits "finish" (f) and "start" (s) martensitic transformation temperatures were determined to be $T(M_f) = 36°C$ and $T(M_s) = 166°C$. The M_f temperature of ZrPd was found to be 550°C. The higher M_s temperature was not observed but ZrPd would be expected to assume the CsCl type structure above the M_s temperature. ZrRh at R.T. behaves like TiNi between its M_s and M_f temperatures. The ZrRh M_s temperature is 380°C above which the CsCl type structure is formed. ZrRu is above its M_s temperature at R.T.; therefore, it has the CsCl type structure. Since A. Raman and K. Schubert[30] have found the ZrRh structure to be of ZrIr type, the ZrIr structure may prove to undergo the same sort of crystal structure changes as TiNi. ZrPt may also behave in a similar fashion and assume a CsCl type structure at a higher temperature.

The alloy system of Zr-Ru and Zr-Os have been established as reported

in Table VI where detailed structures are given. The Zr-Rh system, however, bears some comment. The Zr_3Rh structure [cF112; $E9_3$; CFe_3W_3; a = 3.54Å] reported by C. J. Raub and C. A. Anderson[31] has been disregarded because the structure is common to C, N, O contaminated alloys and the later works of S. T. Zegler[32] and A. Raman and K. Schubert[30] did not produce this structure. The structure of Zr_2Rh which has remained undetermined for some time[30,33] has finally been determined by Zegler.[32] There is a possibility that high and low temperature forms do exist at this stoichiometry which would explain why the phase was not recognized in References 30 or 33. F. E. Wang[29] has cleared up the ZrRh structure as stated above. $Zr_{45}Rh_{55}$ with an undetermined structure reported in reference 30 may belong to the same problem discussed by Wang; this structure is not included in Table VI. A. Raman and K. Schubert[30] were uncertain of a Zr_3Rh_4 phase [cF112, $E9_3$, CFe_3W_3; a = 12.46Å] and thought it may be an oxygen contaminated phase; it is not listed in the table. The Zr_3Rh_5 phase will probably have a free energy of formation much closer to the $ZrRh_3$ phase than indicated in the table; for the Zr_3Rh_5 phase is a distorted cubic structure. The Ti_2Ni type structure of Zr_2Ir has been shown to definitely contain oxygen.[33,34]

The ZrPd structure unidentified in References 35 and 36 has been identified by Wang[29] as TiNi type. The Zr_2Pt_3 phase would be expected to be $MoSi_2$ type while the Zr_4Pt_5 phase is probably a special ordered structure. The Zr_3Ag phase reported by N. Karlson[37] as [tP4; $L6_0$; $CuTi_3$; a = 4.566Å, C = 3.986Å] has not been included; the more recent evidence presented by J. O. Betterton, Jr. and D. S. Easton[38] indicates that it does not exist. The only phase of the Zr-Au system reported in the literature but not included in Table VI is Zr_5Au_4 whose structure was not determined.[35]

V. LITERATURE SURVEY OF SIMILAR SYSTEMS

The high stability of intermetallic binary compounds made from transition metals which has been predicted by Leo Brewer[3] has also been verified by the work of other researchers. Their results follow.

A. The Stability of Zr, Hf, and Th Compounds

J. M. Criscione et al.[20] reacted ZrB_2 and HfB_2 with Rh and Ir as indicated in Table VII. The starting materials were mixed powders. The reaction occurred by sintering in an induction furnace. Differential thermal analysis was used to detect the minimum temperature at which the reaction would support itself exothermally. The samples were then heated under vacuum for 1/2 hour at 1430°C. X-ray analysis of the samples indicated that some boron had dissolved in the reported AB_3 matrices: $ZrRh_3$, $ZrIr_3$, $HfRh_3$ and $HfIr_3$; how much boron is not known because the lattice parameter (a_o) as a function of B has not been determined. Although excess boron was present, only the AB_3 phases could be distinguished from a rather complicated x-ray pattern; the elemental phases of B and Rh or Ir could not be indexed even though the patterns were compared to those of the reactants.

With the access of Rh or Ir present, as given in Table VII, the products might well be Rh or Ir, B and one of the AB_3 phases. Assuming that this is the case, then limits on the ΔF_f of the AB_3 compounds can be determined. From the reaction

$$ZrB_2 + 3Rh \rightarrow ZrRh_3 + 2B,$$

it can be stated:

$$\Delta F^\circ_{rx} \leq 0$$

and

$$\Delta F_f(ZrRh_3) \leq \Delta F_f(ZrB_2) = -76.95 \text{ kcal/mole at } 298^\circ K.^{10}$$

Similar reactions can be written for $ZrIr_3$, $HfRh_3$, and $HfIr_3$; the appropriate limits are given in Table XI. The value of $\Delta F_f^\circ(HfB_2)$ was obtained from R. Hultgren et al.[10] Because B and the excess Rh or Ir were not observed as reaction products, there remains some uncertainty although the reactions appear quite probable.

J. M. Criscione et al.[20] observed reactions of HfC and ThC_2 as well as ZrC with Rh and Ir (Table VIII). The authors proposed reactions which would give C as a product although no mention is made of observing it. The times and temperatures are not given for each reaction, but it can be assumed that 1/2 hour at approximately 2000°C was used. The ThC_2 + Rh sample melted at 1900°C and the room temperature x-ray diffraction pattern could not be identified. The ΔF_f° (HfC), ΔF_f° (ThC_2,γ), and ΔF_f° (ThC,γ) are given by R. Hultgren et al.[10] as -51.6 kcal/mole at 298°K, -22.5 ± 2 kcal/mole at 2600°K, and -23.8 ± 2.9 kcal/mole at 1173°K respectively. ΔF_f° (ThC_2,γ) and ΔF_f° (ThC,γ) are estimated as -23.8 ± 6.5 kcal/mole and -23.8 ± 2.9 kcal/mole respectively at 298°K for the tabulated ΔF_f°'s in Table XI . ΔF_f° (ThC_2 γ) was calculated at the melting point of Th, 2028°K, to be -23.8 kcal/mole assuming that $\Delta S_f^\circ = \Delta S^\circ_{\text{fusion, m.p}}$ (Th) = -1.9 cal/deg. mole of Th between 2600°K and 2028°K. The error limit was increased to account for a ΔS_f° of ± 0.5 cal per degree per gram atom and the ΔC_p° of formation was assumed to be zero. The ΔF_f° (ThC, γ) at 298°K was assumed to equal the 1173°K value and the error limit was broadened as above. The last reaction in Table VIII reported by N. H. Krikorian et al.[39] would indicate that $ThAu_3$ is more stable than ThC. Although some reaction had definitely occurred, there was some doubt expressed by the authors as to whether or not they had actually observed the $ThAu_3$ phase.

B. The Stability of Nb and Ta Compounds

Larry Kaufman[40] observed reactions of NbC with Re, Ru, Ir and Pt; they are reviewed in Table IX. The presence of the $NbRe_{3\pm x}$ was not certain. Since no reaction was observed when NbC and Ru were heated, nothing can be said about the stability of Nb-Ru compounds. The reactions of Re and Ir are most likely energetically favorable at 1200°C as well as at higher temperatures because ΔF_{rx}'s for solid state reactions are quite insensitive to temperature, but they did not occur because the time duration was not long enough at the lower temperature. The limits on the Gibbs free energy of formation derived from these reactions are quite insensitive to temperature, but they did not occur because the time duration was not long enough at the lower temperature. The limits on the Gibbs free energy of formation derived from these reactions and listed in Table XI are based on the ΔF_f° (NbC) given by R. Hultgren.[10]

Peter Riesenfeldt[41] observed a reaction between TaC and Pt yielding $TaPt_3$ as given in Table IX. After hot pressing for 1/2 hour at both 1400°C and 1600°C, an equimolar mixture was observed to contain C, TaC and $TaPt_3$ phases indicating that the C-Ta-Pt ternary phase diagram is similar to the one presented in Fig. 1. From the value of ΔF_f° (TaC) given by R. Hultgren, the $\Delta F_f^\circ(TaPt_3)$ must be lower than -35 kcal/mole at 298°K.

N. H. Kirkorian et al.[39] have determined part of the C-Ta-Re phase diagram at 2700°C. In the Ta-Re binary system, the χ phase $TaRe_{3\pm x}$ extends from 60 to 80 at.% Re[28]. The Re rich end of the χ phase is in equilibrium with $TaC_{0.94}$ and the Re phase. The Ta rich end of the χ phase is in equilibrium with $TaC_{0.70}$ and the Ta phase with 45 at.% Re in solution. The ΔF_f° ($TaRe_{3\pm x}$) is not given because of its wide composition range; the ΔF_f° ($TaRe_{3\pm x}$) will vary over this range.

C. The Stability of U Compounds

N. H. Krikorian et al[39] have observed reactions of ThC, UC, and UN with Ir, Rh, and Au. The ThC reaction with Au was discussed earlier. The reactions of UC and UN are listed in Table X. The reactions were run with cold pressed powders. Based on the reactions of Au with UC and UN, limits on the ΔF_f° (UAu_3) were assigned as:

$$-25 \text{ cal/mole} \geq \Delta F_f^\circ (UAu_3) \geq -50 \text{ kcal/mole.}$$

Table XI compiles the Gibbs free energy of formation of the compounds listed in Table XI. The melting points of U_2IrC_2 and U_2Ir_3 were determined to be 1930 ± 20°C and 2005 ± 20°C, respectively.

D. The Stability of Pt Compounds

E. D. Eastman[64] et al. found that CeS reacts with Pt to give $CePt_2$: $4\ CeS + 2Pt \rightarrow CePt_2 + Ce_3S_4$. M. W. Evans[65] reported the heats of formation of CeS and Ce_3S_4 based on the heat of formation of Ce^{+3}, written as ΔH_f° (Ce^{+3}). The values for Ce^{+3} in aqueous solution with HCl used by M. W. Evans have been corrected:[66] ΔH_f° (Ce^{+3}) in 0.1 MHCl aqueous solution is -167.2 kcal/mole, and ΔH_f° (Ce^{+3}) in 1.0M HCl aqueous solution is -166.0 kcal/mole at 298°K. The resultant ΔH_f° ($CePt_2$) at 298°K is on the order of -51 to -61 kcal/mole.

V. N. Bronger and W. Klemm[42] made several Pt compounds: Pt_3Al, $Pt_{13}Al_3$, Pt_3Sc, Pt_5Y, Pt_4La, $Pt_{15}Be$, Pt_3Mg, Pt_7Mg, Pt_2Ca, Pt_7Ca_2, Pt_5Ca, Pt_2Sr, Pt_3Sr, Pt_5Sr, Pt_7Li, and Pt_3Cr. The non-precious metal oxides were reduced in the presence of Pt and H_2 gas decomposed from NH_3. The crystal structures and lattice constants of the compounds are discussed. The Gibbs free energies of formation could be estimated from the reactions

described in the article, but information additional to that given in the article must first be known or assumed: the flow rate of NH_3 for each run and the weight of each sample before and after heating. The relative weights before and after heating are only given for the Pt-Al and Pt-Sc systems, but total weights are not given for these samples.

Table XI lists the limits of the standard state Gibbs free energies of formation of the various compounds reviewed which are based on the observed reactions with the carbides, the borides, and the nitrides listed in Tables VII to X. The question marks indicate that the various authors have expressed uncertainty in their findings; however, they are probable considering the reactions expressed with certainty. Limits on the standard state free energies of formation of other compounds of a particular binary system can be expressed as they were in Table VI; the necessary steps are outlined in Part III.

Compounds which may prove to be very stable but which have not been investigated to date are those of Sr, Ba, Y and La with Rh, Ir, Pd, Pt Ag, and Au. They too may exhibit high stability. Compounds made from the lanthanide and actinide series are also expected to exhibit high stability due to the availability of low-lying d orbitals. As evidenced by the magnetic susceptibility and the enthalpies of sublimation of these elements, it is probable that f orbitals are not being used for bonding. Combinations of lanthanides and actinides with platinum group metals will most likely form very stable compounds as well.

Caution is advised in carrying out reactions of the nature discussed and in the synthesis of these stable compounds from the elements; the reactions are very exothermic. An explosion while making $HfPt_3$ from the elemental powders has been reported.[4]

VI. DISCUSSION

Table VI and XI summarize the limits of the Gibbs free energies of formation of the various compounds that were obtained and reviewed in this work. Such limits are valuable when very little thermodynamic information is known about the various intermetallic transition element compounds presented. The accurate and more time consuming determination of the free energy of formation of the compounds will be carried out as the need and the interest demand. Their high stability relative to other intermetallic compoundsis strong evidence that the d electrons are actively participating in the bonding. The corresponding bonding character and crystal structures of these compounds can be rationalized by considering the Brewer Predictions.[3]

A striking implication of the high stabilities which were found for these compounds is directly observed in the reactions listed. Refractory carbides are generally chosen for a particular application because of their high melting points and chemical inertness. It has been experimentally verified that these carbides react quite well with Rh, Ir, Pd, and Pt, metals referred to as "noble" because of their chemical inertness.

The oxides are much more stable than the corresponding carbides. It is most probable that the intertransition element compounds are not more stable than the oxides in air. Assuming a ΔF_f° ($ZrPt_3$) of -100 kcal/mole, one can calculate that the partial pressure of oxygen must be less than 10^{-22} atm. before ZrO_2 and Pt will react to form $ZrPt_3$ at 1000°K. Therefore, ZrO_2 and Pt are not expected to react with each other in air or in a vacuum. If a reducing atmosphere such as H_2 were present, the following reaction may occur:

$$ZrO_2 + 3Pt + 2H_2(g) \rightarrow ZrPt_3 + H_2O(g)$$

As derived from reference (43) and from the assumption that ΔF°_f ($ZrPt_3$)= -100 kcal/mole:

$$\Delta F^\circ_{rx} = \Delta F_f(ZrPt_3) + 2\Delta F_f(H_2O) - \Delta F_f(ZrO_2)$$
$$= -100 + 2(-46) - (-205) \text{ at } 1000^\circ K$$
$$= +9 \text{ kcal.}$$

The ΔF°_{rx} may also be expressed as:

$$\Delta F^\circ_{rx} = RT \ln \left(\frac{P_{H_2O}}{P_{H_2}} \right)^2$$

Assuming a P_{H_2} = 1 atm., the partial pressure of $H_2O(g)$ is 0.14 atm. at equilibrium. This calculation implies that the reaction will occur unless the P_{H_2O} is allowed to build up to 0.14 atm. In most reducing furnace atmospheres, it is not allowed to build up to this level. Pt, Pt-Rh thermocouples shielded in ZrO_2 ceramic tubes have been used in furnaces with reducing atmospheres. They were found to become brittle and useless for such runs. This attack was attributed to hydrogen embrittlement for some time, but it can be seen from the above calculation that the brittle $ZrPt_3$ and $ZrRh_3$ phases were being formed.

VII. SUMMARY

The reactions experimentally observed to occur and reviewed are presented in Tables II, III, IV, VII, VIII, IX, and X. The activity coefficients for Zr in Ru, Os, Rh, Ir, Pd, Pt, Ag and Au were determined from the three phase euqilibria involving C and ZrC; they are presented in Table V. The values and limits for the Gibbs free energies of the various compounds discussed are given in Tables VI and XI.

In the C-Zr-Re system the C, the ZrC, and the Re phases were observed to exist in equilibrium. The Re phase was analyzed and found to contain a molar ratio of Zr to Re of 19.0 to 81.0. The % C dissolved in the phase was not determined. The lattice parameters of the Re hexagonal phase had expanded to $a_o = 2.781 \pm 0.004$Å and $c_o = 4.4590 \pm 0.008$Å.

APPENDIX A: Notes on the Engel Correlation and the Brewer Predictions

A. INTRODUCTION

An understanding of the metallic correlation proposed by Neils Engel and experimentally verified by Neils Engel and Leo Brewer can be achieved by predicting crystal structures. The paper, "Viewpoints of Stability of Metallic Structures,"[1] describes how the stability of various crystal structures can be predicted for the metallic elements. It is assumed that the basic ideas of the Engel Correlation are understood by the reader. References 1 and 2 will be particularly helpful. The purpose of this appendix is to consider an example of the Engel Correlation in use. The bcc and hcp crystal structures of niobium are considered. The energy difference between these two structure is determined using the Engel Correlation and the Brewer Predictions at various levels of sophistication. The author hopes that the reader following this example will understand more fully the significance and some of the fine points of the correlation and the predictions presented in all of the papers on these subjects to date.[1-9] It is hoped that those who have a minimum knowledge of thermodynamics will understand the Engel Correlation and the Brewer Predictions after reading the appendix.

Niobium is chosen as the example because it is briefly discussed in Ref. 1 and because it is an element. Both W. Hume-Rothery, and Niels Engel have correlated crystal structure with the electron to atom (e/a) ratio. Crystal structure also depends upon size ratio and the range of composition of a crystal structure is influence by differences in internal pressures and charge transfer. If the Engel Correlation is to be discussed in the simplest possible terms, the contribution of all of these additional factors must be negligible. In a crystal of an element, all atoms are the same size, all atoms have the same internal pressure, and there is no charge transfer; the crystal structure of an element is the logical place to start.

B. Nb(bcc) → Nb(hcp) USING INTEGRAL LIMITS

Predicting the relative stability of the crystal structures of Nb implies that the free energy can be determined for the reaction:

$$Nb(bcc) \xrightarrow[\Delta F_{rx}]{} Nb(hcp)$$

Recalling from thermodynamics, if $\Delta F_{rx} < 0$, then Nb(hcp) is the stable structure; if $\Delta F_{rx} > 0$, then Nb(bcc) is the stable structure; and if $\Delta F_{rx} = 0$, then the two structures are in equilibrium. The determination of such ΔF_{rx}'s is a principle contribution by Leo Brewer[1] to the Engel Correlation. Choosing a different path does not change a state function; therefore, consider the energy changes associated with going to the monoatomic gas in the ground state, as is represented in Fig. 6. The bcc structure of Nb is correlated to an electronic configuration of $4d^4 5s^1$, or an e/a ratio equal to 1 considering only the metallic electrons of Nb, i.e., s and p electrons. The hcp structure correlates to an e/a ratio of 2. These integer values of e/a ratios correlated to crystal structure represents the first level of sophistication of the Engel Correlation. (The fcc or ccp structure correlates to 3 electrons per atom.)

ΔF°_{rx} can be calculated knowing the values for the various state functions presented in Fig. 6. $\Delta H_{\text{atomization } ①}$, i.e. for bcc Nb, has been determined experimentally and is given in Table VI of Ref. 1 as +173 kcal/mole. Since the main species of vaporizing Nb is monoatomic gas, $\Delta H_{\text{atomization } ①} = \Delta H_{\text{sublimation } ①}$. This equality holds only if the solid sublimes to monoatomic gas. $\Delta H_{\text{atomization}}$ can otherwise be calculated knowing the dissociation energies involved and the sublimation energy. Figure 7 illustrates this point. $\Delta H_{\text{atomization } ②}$ is not

known experimentally because the hcp structure of Nb has not been observed. Since $\Delta H_{atom\,(2)}$ is a state function, it may be determined knowing $\Delta H_{prom\,(2)}$ and $\Delta H_{bond\,(2)}$. (See Fig. 6.) $\Delta E_{prom(2)}$ is given in Ref. (1) as +48 kcal/mole; both electronic states have been observed. The $(d^3s^1p^1)$ excited electronic configuration corresponds to the atomic orbital occupancy associated with hcp Nb. Crystallizing from this excited state involves bonding directly three-d-type electrons and two s,p-type electrons. The bonding energies of these electrons are given in Fig. 8, a reproduction of Fig. 2, Ref. (1). $\Delta H_{bond(2)} = n_dE_d + n_pE_p$ where $n_d \equiv$ number of bonding d electrons, $E_d \equiv$ bonding enthalpy per d electron (E_d is the function of n_d), $n_p \equiv$ number of bonding s and p electrons, and $E_p \equiv$ bonding enthalpy per s and p electron (E_p = function of atomic number). From Fig. 8, $\Delta H_{bond\,(2)} = n_dE_d + n_pE_p =$ $3(-35\ 1/4 + 2(-51\ 2/3) = -210$ kcal/mole.

From the above discussion $\Delta H_{atom\,(2)}$ and ΔF°_{rx} can now be calculated:

$$\Delta H_{atom\,(2)} = -(\Delta E_{prom\,(2)} + \Delta H_{bond\,(2)}) =$$
$$= -(+48 - 210)$$
$$= +162 \text{ kcal/mole}$$
$$\Delta F^\circ_{rx} = \Delta H_{atom\,(1)} - \Delta H_{atom\,(2)}$$
$$= +173 - 162$$
$$= +11 \text{ kcal/mole}$$

The standard state superscript ($^\circ$) on ΔF_{rx} indicates that the calculation is made for the two forms of Nb not being alloyed.

In Fig. 6, ΔF, ΔH, ΔE values have been used interchangeably as in Ref. (1). It may not be immediately obvious that this is legitimate. From elementary thermodynamics, $\Delta H = \Delta E + P\,\Delta V$ for constant pressure reactions. Since there is no volume change associated with the promotion of one mole of a gas from one electronic configuration to another, $\Delta E_{prom} = \Delta H_{prom}$. Also,

$\Delta F = \Delta H - T\Delta S$ for constant temperature reactions. The difference in entropy between two solid structures where all electrons are tightly bound is negligible, about ±1 e.u. or less (e.u. ≡ entropy unit = cal/mole degree). To within ±1 kcal/mole per 1000°K, $\Delta F^\circ_{rx} = \Delta H^\circ_{rx}$. Therefore, all state function represented in Fig. 6 are enthalpies. All reactions in Fig. 6 may take place at any one temperature; all gases may be at any single pressure. The calculations are made for unalloyed solid structures and at one atmosphere pressure as designated by the standard state superscript ($^\circ$). The vaules from Ref. (1) are taken at 298°K.

One important question remains: From where do curves like those represented in Fig. 8 used to obtain $\Delta H_{bond\,②}$ come? Consider the three-reaction cycle designated by ① in Fig. 9. In this case $\Delta H_{atom\,①}$ and $\Delta E_{prom\,①}$ are known experimentally. $\Delta H_{bond\,①}$, equal to $-(\Delta H_{atom\,①} + \Delta E_{prom\,①})$, is -173 kcal/mole. ($\Delta E_{prom}$ is included because it may not always equal zero). $\Delta H_{bond\,①}$ is therefore obtained experimentally. ΔH_{bond} has been obtained for all elements in the transition series where ΔH_{atom} and ΔE_{prom} are available, i.e. where crystal structures are observed and where spectroscopic data have been obtained for the electronic states involved. Elements which have no d electrons bonding, such as Sr (hcp) and Cd(hcp) help determine the E_p versus atomic number curve. E_p increases with increasing atomic number rapidly at first and then more slowly reflecting the corresponding trend in atomic radii. The E_d versus n_d curve is obtained by difference. The final curves represent the best fit for all elements considering this interplay of E_p and E_d.

An important feature of these curves is that the energy per d electron is not a function of crystal structure. The curve E_d vs. n_d for bcc structures lies on top of the curve for hcp. Although the curve was obtained using ΔH_{atom} for one crystal structure of an element [$\Delta H_{atom\,①}$

for Nb (bcc)], it may be used to find $\Delta H_{bond\ ②}$, and therefore $\Delta H_{atom\ ②}$ for another crystal structure of an element [$\Delta H_{atom\ ②}$ for Nb (hcp)]. The fact that E_d versus n_d gives a curve and not an array of points provides support to the Engel Correlation and the Brewer Predictions. The actual shapes of the curves are discussed by Brewer elsewhere.[1,2]

These are the important features of the Brewer Predictions. It has been used to predict that hcp Nb is unstable by 11 kcal/mole. Not only does this imply that bcc Nb is expected to be observed but it also implies that hcp Nb is not expected to be thermodynamically stable at any temperature or pressure. The change in ΔF_{rx} with temperature is given by $\Delta F_{rx} = \Delta H_{rx} - T\Delta S_{rx}$. Assuming a $\Delta S^\circ_{rx} = +1$ e.u., a temperature of 11,000°K would be needed to overcome the +11 kcal/mole free energy of reaction at 298°K. Nb melts well before this temperature is reached. The change in free energy with pressure is given by $\Delta F_{rx} = \int^x \Delta V_{rx}\, dP \sim \Delta V_{rx} \Delta P$. Assuming a value of $\Delta V^\circ_{rx} = -5$ cc/mole, 91,000 atm. would be necessary to overcome the 19 kcal/mole energy difference. These values of ΔS°_{rx} and ΔV°_{rx} represent the hypothetical extremes that would favor a conversion to the hcp structure.

C. NONINTEGRAL VALUES FOR ELECTRONIC STATES

In the previous example, the Engel Correlation has been used in its simplest form; the crystal structures in question have been correlated to integral values of electron per atom ratios, such an atomic orbital approach is not an adequate method of describing crystal bonding. More sophisticated bonding schemes, however, can be represented as combinations of the former. The resultant atomic orbital scheme would have nonintegral values, such as ($4d^{3.9}5s^{1.0}5p^{0.1}$) for Nb. Such an electronic configuration does not imply that 90% of the Nb atoms in the crystal have the ($3d^{4}5s^{1}$) configuration and 10% have the ($3d^{3}5s^{1}5p^{1}$) configuration; it does imply that each Nb atom in the crystal has the same electronic configuration, one expressed in a configuration more complicated than that given by atomic orbital theory but one that can be expressed as a combination of atomic orbitals as presented. The total number of electrons per atom must remain integral, however, as long as no charge transfer occurs.

D. Nb MODEL USING NONINTEGRAL LIMITS

Ignoring the simplifying restraint of using electron to atom ratios of whole numbers, the configuration of lowest energy for Nb will now be determined. Referring to Fig. 9, such a configuration will exist when ΔH_{atom} for that configuration is at a maximum or when $\partial\Delta H_{atom}/\partial n_d = 0$. A change to any other configuration would be accompanied by a positive free energy of reaction.

The most stable configuration is obtained by solving for the number of bonding d electrons per atom of the configuration. Two equations are used: (a) $n_d = [E_{prom} - (E_p - E_d)]/S$, Eq. (6), which is given by the condition $\partial\Delta H_{atom}/\partial n_d = 0$; and (b) $E_d = a - S(n_d)$ which is derived from the E_d versus n_d curve of Fig. 8. Their derivations follow.

Derivation of: $n_d = [E_{prom} - (E_p - E_d)]/S.$ (6)

From Fig. 9:

$$\Delta H_{atom} = -(\Delta E_{prom} + \Delta H_{bond}) \tag{4}$$

$$-\Delta H_{atom} = +\Delta E_{prom} + n_p E_p + n_d E_d$$

Differentiating:

$$\frac{-\partial\Delta H_{atom}}{\partial n_d} = \frac{\partial\Delta E_{prom}}{\partial n_d} + n_p \frac{\partial E_p}{\partial n_d} + E_p \frac{\partial n_p}{\partial n_d} + n_d \frac{\partial E_d}{\partial n_d} + E_d \tag{5}$$

n_d: n_d is defined as the number of d electrons in a particular electronic configuration. For $n_d < 5$, the number of d electrons available for bonding is equal to the total number of d electrons, n_d. For $n_d > 5$, the number of bonding d electrons is $10 - n_d$. The abscissa in Fig. 8 is the

number of unpaired d electrons or the number of d electrons available for bonding and is not n_d.

$\frac{\partial(\Delta E_{prom})}{\partial n_d}$: The first term in Eq. (5) is the change in promotion energy between two electronic states differing by the number of d electrons. Let E_{prom} be defined as $\frac{\partial(\Delta E_{prom})}{\partial n_d}$. In the case of Nb,

$$E_{prom} = \frac{\partial \Delta E_{prom}}{\partial n_d} = \frac{\Delta E_{prom}\,(d^3s^1p^1) - \Delta E_{prom}\,(d^4s^1)}{3-4} = +\,48/(3-4) = -48 \text{ kcal/mole.}$$

$\frac{\partial E_p}{\partial n_d}$ and E_p: As mentioned previously E_p is not a function of n_d but is a function of atomic number; therefore $\partial E_p/\partial n_d = 0$. For Nb, the bonding energy per p electron, E_p, is $-51\frac{2}{3}$ kcal/mole.

$\frac{\partial n_p}{\partial n_d}$: The number of s and p electrons is related to the number of d electrons because the total number of electrons per atom remains the same as the configuration changes. This is true only when no charge transfer occurs. $n_p = n_{total} - n_d$; therefore $\partial n_p/\partial n_d = -1$.

$\frac{\partial E_d}{\partial n_d}$: Reference (1) defines the term "S" as "the rate of change of E_d with decrease in the number of d electrons;" therefore, $S = -\partial E_d/\partial n_d$. $\partial E_d/\partial n_d$ can be calculated from the slope of the E_d versus n_d curve in Fig. 8. For Nb, S = -6.8 kcal/mole.

Summing up the above and setting $\partial \Delta H_{atom}/\partial n_d = 0$, Eq. (5) becomes:

$$\begin{aligned} 0 &= E_{prom} - E_p - n_d\,S + E_d \\ n_d &= [E_{prom} - (E_p - E_d)]/S \end{aligned} \qquad (6)$$

Using the values for Nb as discussed above, one would obtain the following equation for Nb:

$$n_d = [-48 - (-51\tfrac{2}{3}) + E_d]/-6.8$$
$$= -\frac{(3.67 + E_d)}{6.8} \qquad (7)$$

The values for Nb as discussed above are all negative numbers. The remaining bonding enthalpy, E_d, is also negative since it is the enthalpy lost by the system as the bond is formed. If the solid were taken as the zero enthalpy reference level, then the numbers used would all be positive and the answer would remain the same:

$$n_d = [+48 - (+51\tfrac{2}{3}) + E_d]/(+6.8)$$
$$= \frac{-3.67 + E_d}{6.8}$$

where E_d is a positive number. The only difference between the two methods is the sign convention. In the first case, all values used are thermodynamically correct, i.e. the bonding enthalpy is the energy change of the system as the bond is formed; it is a negative number. Leo Brewer in Ref. (1) preferred the latter convention so that all values used in Eq. (6) would be positive numbers, thus making the arithmetic easier. In order to help straighten out the sign conventions, they are outlined below and the reader is free to use whichever he feels more suitable.

A. If ΔH_{bond} is a negative number:

(1) then all of the values used in Eq. (6) will be negative because of the following consequences of (A).

(2) E_p, defined as the bonding enthalpy per p electron, will be negative. For Nb, $E_p = -51\frac{2}{3}$ kcal/mole.

(3) E_{prom} will equal $\partial(\Delta E_{prom})/\partial n_d$. ΔE_{prom} is the promotion energy associated with any excitation and ∂n_d describes the corresponding change in the number of d electrons. For Nb,

$$\frac{\partial(\Delta E_{prom})}{\partial n_d} = \frac{+48-0}{3-4} = -48 \text{ kcal/mole.}$$

(4) $\partial n_p/\partial n_d = -1$

(5) Let $S \equiv -\partial E_d/\partial n_d$. For $n_d < 5$, the slope, $\partial E_d/\partial n_d$, is positive because E_d is a negative number. For Nb, $S = -\partial E_d/\partial n_d = \frac{-29.2 - (-36)}{4-3} = -\frac{+6.8}{+1} = -6.8$ kcal/mole.

(6) The unknown, E_d, is a negative number.

B. If all values to be used in Eq. (6) are to be positive a priori:

(1) then ΔH_{bond} will be a positive number

(2) E_p will be a positive number

(3) $\partial\Delta E_{prom}/\partial n_d$ is still a negative number but E_{prom} is defined as "the energy to promote a d electron" to a p electron. Therefore, $\Delta n_p = +1$, $\Delta n_d = -1$, and $E_{prom} = -\partial(\Delta E_{prom})/\partial n_d$.

(4) $\partial n_p/\partial n_d = -1$.

(5) Let $S \equiv -\partial E_d/\partial n_d$. For $n_d < 5$, the slope will now be negative and S will be positive. For Nb, $S = -\frac{\partial E_d}{\partial n_d} = -\frac{+29.2 - (+36)}{4-3} = -[-6.8] = +6.8$ kcal/mole.

(6) The unknown, E_d, will be a positive number.

Derivation of: $n_d - 5 = [E_{prom} - (E_p + E_d)]/S$.

Leo Brewer[1] has given an equation similar to Eq. (6) for $n_d > 5$. Since it is in error,[60] it will also be derived.

As before:

$$\Delta H_{atom} = -(\Delta E_{atom} + \Delta H_{bond})$$

$$-\Delta H_{atom} = \Delta E_{prom} + n_p E_p + (10-n_d)E_d$$

Differentiating

$$-\frac{\partial\Delta H_{atom}}{\partial n_d} = \frac{\partial\Delta E_{prom}}{\partial n_d} + E_p \frac{\partial n_p}{\partial n_d} + n_d \frac{\partial E_p}{\partial n_d} - (10-n_d) \frac{\partial E_d}{\partial n_d} + E_d(-1) \qquad (8)$$

The terms defined for Eq. (6) also hold for Eq. (8). Setting $\partial\Delta H_{atom}/\partial n_d = 0$, Eq. (8) becomes:

$$0 = E_{prom} - E_p - (10-n_d)\, S - E_d$$

$$10-n_d = \frac{E_{prom} - (E_p + E_d)}{S} \qquad (9)$$

The sign conventions expressed for Eq. (6) are also true for Eq. (8) with one exception in each case:

Case A. S, assuming its sign from the accepted convention that ΔH_{bond} is negative, will be positive in this case.

Case B. S is <u>not</u> assumed to be positive a priori. $S = -\partial E_d/\partial n_d$ as before. For $n_d > 5$, the slope will be positive because E_d is positive by this convention. S will be negative.

<u>Derivation of: $E_d = a + (\partial E_d/\partial n_d)\, n_d$.</u> (10)

It is evident from Fig. 8 that E_d can be expressed as a linear function of n_d over a range of $\Delta n_d = 1$. Such a linear function is expressed mathematically as Eq. (10) where a is a constant.

<u>Optimum Configuration for Nb:</u>

Using Eqs. (6) and (10) derived above, the optimum configuration for Nb can be calculated. The sign convention chosen for the problem will conform with ΔH_{bond} being a negative number. Equation (6) was reduced to Eq. (7) using the appropriate values for Nb:

$$n_d = -\frac{(3.67 + E_d)}{6.8} \qquad (7)$$

As discussed earlier, $\partial E_d/\partial n_d = +6.8$. The constant used in Eq. (10) can be evaluated by noting that $E_d = -36$ kcal/mole when $n_d = 3$. Equation

(10) becomes:

$$E_d = -56.4 + 6.8\ n_d \qquad (11)$$

Equations (7) and (11) represent the two equations necessary to solve the problem for the two unknowns. Setting Eqs. (7) and (11) equal:

$$E_d = E_d$$

$$-3.67 - 6.8\ n_d = -56.4 + 6.8\ n_d$$

$$n_d = +\frac{52.7}{13.6} = 3.9$$

Therefore, the configuration of minimum energy for Nb is $(4d^{3.9}5s^{1.0}5p^{0.1})$.

Using this value in Eqs. (7) or (11) gives E_d = -30.1 kcal/mole.

Refinements in the Brewer Predictions

The Brewer Predictions are refined on two accounts from calculations like the one above. As mentioned in the integral electron to atom ratio model for Nb, ΔH_{bond} is calculated knowing ΔH_{atom} and ΔE_{prom} for the particular crystal structures observed and for the assumed electronic configurations for the elements. The assumed electronic configurations can now be nonintegral, for example $(4d^{3.9}5s^{1.0}5p^{0.1})$ for bcc Nb. That is to say, using the integral ratio curves and Eqs. (6) and (10), a more refined set of curves could be generated. As it turns out, the refined curves fall on top of the integer model curve and Fig. 8, as reproduced from Ref. 1, is made up of integral and nonintegral electronic configurations. Going from left to right, the electronic configurations represented by the bcc structure are: Sr $(4d^{0.5}5s^{1.0}5p^{0.5})$, Y$(4d^{1.5}5s^{1.0}5s^{0.5})$, Y$(4d^{2.0}5s^{1.0})$, Zr$(4d^{2.5}5s^{1.0}5p^{0.5})$, Zr$(4d^{3.0}5s^{1.0})$, Nb$(4d^{4.0}5s^{1.0})$, and Mo$(4d^{5.0}5s^{1.0})$. The electronic configurations corresponding to the hcp structures are Y$(4d^{1.0}5s^{1.0}5p^{1.0})$, Y$(4d^{1.3}5s^{1.0}5p^{0.7})$, Zr$(4d^{2.0}5s^{1.0}5p^{1.0})$, Zr$(4d^{1.3}5s^{1.0}5p^{0.7})$, Tc$(4d^{5}5s^{1.0}5p^{1.0})$, and Ru$(4d^{1.4}5s^{1.0}5p^{0.6})$.

Sr(hcp $5s^{1.0}5p^{1.0}$) accounts for the point: E_p = -40 kcal/mole, n_d = 0.

As drawn, Fig. 8 is difficult to read to the accuracy which can be used with these calculations. Table XII lists the values of n_d, E_d, and E_p associated with the various elements from the refined calculations. Some of the values were calculated from the experimentally observed thermodynamic quantities, such as the Nb (bcc) values. The values calculated from the refined curves for unobserved structures are also given, such as for Nb(hcp). These values may be used to draw a more accurate set of curves than those of Fig. 8. The accuracy of the final atomization enthalpy (ΔH_{atom}) calculated from the bonding energies of Table XII and the appropriate promotion energies is accurate to ±1 kcal/mole of element.

The second refinement in the Brewer Predictions concerns the metallic electron to atom ratio limits for the crystal structures. The optimum electronic configuration for the metallic elements was found at the same time that the refined curves of Fig. 8 were found. The crystal structures of the corresponding elements have been determined experimentally. The resultant empirical correlation aided in determining the limits used by Leo Brewer as presented in Table XIII(a). Structures from multicomponent systems were also used to determine the limits. As discussed earlier, several factors contributed to the crystal structures of multicomponent systems. The Brewer limits are narrower than those presented by Niels Engel (Table XIII(b)). The Brewer limits represent electron to atom ratios where the free energy of the phase in question has been found to rise sharply. The observed empirical limit would depend upon the energy of the other structures in the phase diagram. The limits are also an attempt to express only the electron to atom effect upon crystal structure and to avoid the other factors. Neils Engel's limits, on the other hand, are

more empirically based and he has attempted to cover small changes in the other factors by giving broader electron to atom limits.

Nb(bcc) → Nb(hcp) Using Nonintegral Limits

Knowing these limits and the configuration of minimum energy for the most stable crystal structure of an element, a more accurate free energy difference between two crystal structures of the same element can be calculated. Again Nb can serve as an example:

$$Nb(bcc,\ 4d^{3.9}5s^{1.0}5p^{0.1}) \xrightarrow[\Delta F^{\circ}_{rx}]{} Nb(hcp,\ 4d^{3.3}5s^{1.0}5p^{0.7})$$

The configurations chosen indicate a reaction from niobium's most stable structure to the point of highest stability for the hcp structure.

The experimentally observed ΔH_{atom} for bcc pertains to its most stable configuration: ΔH_{atom} ① = +173 kcal/mole. Referring to Fig. 10, ΔH_{atom} ② can be calculated knowing ΔE_{prom} ② and ΔH_{bond} ②. ΔE_{prom} ② is equivalent to promoting 70% of the atoms to the $(4d^{3}5s^{1}5p^{1})$ state and leaving 30% in the ground state $(4d^{4}5s^{1})$. ΔE_{prom} ② = (0.7)(+48) = 33.6 kcal/mole.

ΔH_{bond} ② is obtained from Fig. 8 or Table XII

$$\Delta H_{bond} ② = n_p E_p + n_d E_d$$
$$= (1.7)(-51\tfrac{2}{3}) + (3.3)(-33) = -197 \text{ kcal/mole}$$

Solving for ΔF°_{rx}

$$\Delta H_{atom} ② = -(+33.6 - 197) = +163 \text{ kcal/mole}$$
$$\Delta F^{\circ}_{rx} = +173 - 163 = +10 \text{ kcal/mole}$$

As would be expected from the calculations, only bcc Nb has been observed to date.

All the elements for which the Engel Correlation apply, namely metallic solids, can be treated in a similar manner. Reference 1 sketched out the steps covered in greater detail above for Nb; another example was Zr. The change in free energy for Zr (bcc) → Zr (hcp) is very close to zero indicating that both bcc and hcp Zr can be expected with changes in temperature and pressure. This is experimentally verified.

The promotion energies of interest are those corresponding to energy differences between the ground electronic configuration and the $d^{n-1}s$, $d^{n-2}s^1p^1$, $d^{n-3}s^1p^2$ configurations of gaseous atoms. Unfortunately, the promotion energies for the $d^3s^1p^2$ configuration of the elements are not known; however, this approach has been successful in predicting whether or not the unstable bcc or hcp crystal structure of an element will ever be observed.

E. PREDICTION OF THE CHANGE IN CRYSTAL STRUCTURE WITH PRESSURE

Leo Brewer's predictions of the stability of crystal structures is based on simple thermodynamics. If one accepts that the bcc structure and the hcp structure are correlated to less than 1.5 s,p electrons and more than 1.7 s,p electrons, respectively, then for the transition metals to the left of Group 7, the bcc structure has more bonding d electrons than does the hcp structure. Anything which improves d electron bonding will then stabilize the bcc structure over the hcp structure. Experience with the intermetallic compounds, indicate that d electron overlap is poor compared to overlap in s,p bonds and compression of the phase to decrease internuclear distances favors d bonding over that of s,p bonding. On the basis of these two correlations, one predicts that the bcc structure will be stabilized by pressure relative to hcp for transition metals of the left hand side of the periodic table. Exactly the same argument predicts the reverse behavior for the Seventh Group and beyond to the right; since bcc structure will have more d electrons and therefore less bonding d electrons once one passes the half-filled d configuration.

This prediction can be reconciled with the thermodynamic requirements of volume change. The change in Gibbs free energy associated with volume change is expressed by the relation: $\Delta F = \int \Delta V dP$; the more dense phase is favored by compression. The 8 coordinate bcc structure might be less dense than the 12 coordinate hcp structure, but for the transition elements on the left side, the improved d bonding upon compression will result in higher compressibility for the bcc structure until it becomes more dense than the hcp structure. If the bcc structure is already more dense due to smaller internuclear distances in the structure of lower

coordination number, it will remain stable at elevated pressures. This model gives very reliable results. For multicomponent systems, the problem is easy to handle since many factors cancel in the comparison of the two phases of the same composition.[59]

Zirconium is a prime case in point. The theoretical molar volume ($\bar{v}$) for hcp Zr ($d^{2.3}s^{1}p^{0.7}$) is 14.0 cc/mole; for bcc Zr ($d^{2.5}s^{1}p^{0.5}$), v_{bcc} = 14.2 cc/mole at 600°C, 1 atm as calculated from the lattice parameters.[44] If one did not expect either volume to change with pressure, the hcp structure would be predicted to be stabilized by an increase in pressure. Realizing the d bonds are stabilized, one would predict that v_{bcc} would decrease with an increase in pressure relative to the v_{hcp} and that the bcc structure would be stabilized by an increase in pressure. The latter is actually the case: bcc Zr is stabilized by an increase in pressure. The bcc structure of Ti is also stabilized by an increase in pressure.[59]

The bcc structure must have highly directional forces to maintain itself. At sufficiently higher pressures, these directional forces will be deformed and the situation should become more complicated.

F. PERCENT P-CHARACTER

The concentration limit of the Engel Correlation can also be expressed as percent p-character. Leo Brewer[2] has reported these limits and they are reproduced in Table XIII(a). This representation is simply the number of p electrons divided by the total number of s and p electrons participating in the bonding. The metallic electrons of Nb (bcc) have 9% p-character. Examining the accumulated experimental evidence, it is not obvious whether or not this representation is more definitive of the nature of the metallic bond than the s,p representation.[2]

The advantage of expressing the limits as percent p-character is that certain apparent exceptions to the Engel Correlation could be explained. Face-centered Sr is such a case; without using electrons from the Kr core of filled levels, a configurations of ($5s^{0.5}5p^{1.2}$) would explain this structure.

G. THE ENGEL CORRELATION AND COPPER

Physicists have assigned the ($3d^{10}4s^{1}$) configuration to fcc Cu for some time, the feeling being that this configuration more readily explains the diamagnetic nature of Cu than does the ($3d^{8.5}4s^{1}4p^{1.5}$) configuration assigned to Cu by Engel. Engel has made reference to copper's diamagnetic susceptibility but did not explain it in depth.[6] Comparing the magnetic susceptibility of Cu to other elements in the periodic table can be misleading. All metal elements start with an inner closed shell core of paired electrons contributing a diamagnetic effect to the susceptibility. A paramagnetic effect is added as the outer valence electrons are added. Even if the valence electron are bonded, the application of a magnetic field tends to unpair the bonds slightly and contribute paramagnetically. Since this contribtuion adds to an already negative term, however, no significance can be attached in going from minus to plus susceptibility, i.e. from diamagnetism to paramagnetism. The unpairing of one electron contributes $+5000 \times 10^{-6}$ cgs units to the susceptibility. The difference across the transition series represents a change on the order of 0.1 of an unbonded electron. The Engel Correlation can be used to demonstrate that the ferromagnetic materials, Fe, Co and Ni, do not pair all of their electrons as electron pair bonds, but the model does not provdie a calculation of the number of unpaired electrons for non-ferromagnetic metals with the order of 0.1 or less unpaired electrons per atom.[60]

From the experimental work done on Cu to examine the crystal wave functions near the Fermi surface, it appears to the physicist as though Cu has one valence electron per atom, thus supporting the ($3d^{10}4s^{1}$) configuration. As pointed out by Niels Engel such a configuration would

contradict several macroscopic properties observed for Cu.[6] It is possible that the $(3d^{8.5}4s^{1}4p^{1.5})$ configuration offers such tight bonding even for the metallic (s,p) electrons that only about one electron per atom is observed in some perturbing experimental phenomena.

If the crystal wave functions popular to the physicist were converted to the atomic orbital picture used to describe the Engel Correlation, then agreement or disagreement may more readily be observed. The density of states for the atomic orbitals have not been obtained from the crystal wave functions for Cu to date. This calculation could be done since crystal wave functions are usually generated from atomic orbitals. Robert G. Lye has made such a calculation for TiC.[61] The resultant density of atomic orbital states gives an electronic configuration of $Ti^{-1\ 1/4}$ $(3d^{4}4s^{3/4}4p^{1/2})$ $C^{+1\ 1/4}$ $(2s^{2}2p^{3/4})$ and a charge transfer of electrons from C to Ti. Such a charge transfer indicates that the d electrons are strongly bonding and can compete favorably with octet s,p bonding. The bonding metallic electrons have 63% p-character $[(1\ \frac{1}{4})\ /2]$. Since TiC has a fcc structure it is in agreement with one of the ways of expressing the e/a limits of the Engel Correlation.

There is a basic fault with such a calculation, however, the crystal wave functions are derived to support experimental observations pertaining to the Fermi surface. A density of states calculation is carried out over the entire Brillouin Zone, not just at the Fermi surface. The calculation therefore involves an extrapolation.

Such a calculation for Cu may lead to the $(3d^{8.5}4s^{1}4p^{1.5})$ configuration proposed as a possibility by Neils Engel; or it may lead to a configuration with 60% or more of its metallic valence electrons having p-character; or it may show that the Engel Correlation is truly not supported by the crystal wave function model for Cu. H.L. Davis is presently performing the calculation.[60]

H. FURTHER READING

The above example has been used to explain some of the fine points of the Engel Correlation and the Brewer Predictions. Once the reader has familiarized himself with these basic concepts, he may venture in one of several different directions. Niels Engel has discussed the properties expected from such bonding.[6,7] The main body of this writing experimentally testifies to the stability achieved by d-bonding. W. Hume-Rothery had criticized the Engel Correlation.[8,9] He, Leo Brewer,[2,4] and Neils Engel[6] have discussed some of the apparent exceptions.

Predictions of Multicomponent Phase Diagrams

Multicomponent metallic systems are discussed throughout the various articles. These systems involve several variables, as mentioned earlier; however, one important step in predicting crystal structure is knowledge of its dependence on the electron to atom ratio. The dependence of the other variables and the interdependence of these variables on the crystal structure is more complicated. The only crystal structures presented here were the bcc, the hcp, and the ccp (or fcc) structures; this was done for simplicity. Some of the elements and many multicomponent alloys have other crystal structures. The Engel Correlation and solution theory is being used to predict when all structures are expected to occur and over what range of composition. Leo Brewer's chapter in *High Strength Materials*[3] discusses the occurrence of multicomponent phases in a semiquantitative manner. Larry Kaufman and Harold Bernstein[62] using the Engel Correlation and solution theory have combined the appropriate variables to generate binary and ternary phase diagrams. They have had some success and are continuing their work.

APPENDIX B

Calculation of the ΔF_f° ($ZrAu_4$)

Given: It has been experimentally determined that C(solid) and ZrCl(solid) exist in equilibrium with the Au (liquid, 9.5 ± 3.5 at.% Zr) phase. E. Raub and M. Engel[55] report that 7.1 at.% Zr dissolve into the Au(s) phase at 1000°C.

At 1500°C, since C, ZrC and Au (9.5 ± 3.5 at.%) exist in equilibrium, the a_{Zr} is known as in the cases of the $ZrIr_3$ and the Ru samples.

$$a_{Zr}^{Au} = a_{Zr}^{ZrC} = 10^{-5.191}$$

Since there is such a large error associated with the %Zr in Au, the calculation will be carried out for the lower limit, 6.0 at.% Zr. The calculation for the upper limit of 13.0 at.% is similar. The resulting $\Delta F_f(ZrAu_4)$ will be expressed with the appropriate error.

Since Eq. (2) is going to be used, the internal pressure parameter will have to be determined. The electronic configuration for fcc Au according to the Engel Correlation and the Brewer Predictions is ($5d^8$-$6s^16p^2$). If Zr is to take advantage of the Au bonding in the Au phase, it would take on an electronic configuration of $(4d^25s^15p^2)^{-1}$. Since the charge transfer is to an extra p electron and not an extra d electron, it is not exactly like its 5 valence electron neighbor : Nb (b.c.c., $4d^4\ 5s^1$). By assuming the internal pressure to increase because of the additional bonding p electron, the predicted value is : $[(\Delta E/V)_{Zr^{-1}}]^{1/2}$ = 107 $cal^{1/2}/cc^{1/2}$. The addition of a p electron will not change the volume of Zr by much. An addition of a d electron would decrease the volume because the nearest neighbor bonding would be tighter; this was evidenced

by the Zr in Ru predictions. The volume of Zr is 14.0 cc/mole. The internal pressure of Au will remain unchanged because not enough Zr has been added: $[(\Delta E_{Au}/V_{Au})]^{1/2} = 92\ cal^{1/2}/cc^{1/2}$. The internal pressure parameter for the Zr-Au system at large Au concentrations becomes:

$$\mathcal{C}_{Zr\text{-}Au} = V_{Zr\text{-}1}\left\{\left[(\Delta E/V)_{Zr\text{-}1}\right]^{1/2} - \left[(\Delta E/V)_{Au}\right]^{1/2}\right\}^2$$

$$= 14.0\ (107\text{-}92)^2\ cal.$$

$$= 3150\ cal.$$

Using the 6.0 at.% Zr limit, the γ_{Zr}^{Au} (0% Zr) can be calculated. Using Eq. (1) at 6.0 at.% Zr:

$$\gamma_{Zr}^{Au}\ (6.0\ at.\%\ Zr) = 10^{-5.191}/0.060 = 10^{-5.191}/10^{-1.222}$$

$$= 10^{-3.869}$$

Using Eq. (2) in order to obtain γ_{Zr}^{Au} (0% Zr):

$$\log_{10} \gamma_{Zr}^{Au}\ (0\%\ Zr) = \log_{10} \gamma_{Zr}^{Au}\ (6.0\ at.\%\ Zr) + \frac{(3150)\ (1\text{-}0.94)^2}{(4.575)\ (1773^\circ K)}$$

$$= -3.869 + 0.0452$$

$$= -3.824$$

$$\therefore\ \gamma_{Zr}^{Au}\ (0\%\ Zr) = 10^{-3.824}\ \text{at}\ 1500^\circ C$$

The γ_{Zr}^{Au} (0 at.% Zr) at 1000°C can now be calculated. Consider the reaction:

$$Zr(\text{solid, pure}) \rightarrow Zr(\text{in liquid Au, 0\% Zr})$$

The change in free energy for this reaction (ΔF_{rx}) is also known as the excess partial molar free energy of Zr ($\bar{F}_{Zr}^{xs}$).

$$\Delta F_{rx} = \bar{F}_{Zr}^{xs} = + RT \ln \gamma_{Zr}^{Au}$$

For the reaction, the change in heat capacity will be small and the dependence of ΔF_{rx} upon temperature can be expressed as $\Delta F_{rx} = \Delta H_{rx} - T\Delta S_{rx}$ where ΔH_{rx} and ΔS_{rx} are relatively constant with temperature. ΔS_{rx} can be approximated as an entropy of fusion because one mole of Zr is going from a solid state to a liquid state. Entropies of fusion are usually $\sim +2.3$ cal/deg. mole. Therefore, to the melting point of Au, $\Delta S_{rx} = +2.3$ e.u.

$$\Delta F_{rx}\ (1063^\circ C) - \Delta F_{rx}\ (1500^\circ C) = -\Delta S_{rx}\ (1063 - 1500)$$
$$= -(2.3)\ (-437)\ \text{cal/mole}$$
$$= +1.005\ \text{kcal/mole}$$

ΔF_{rx} at 1500°C can be found because γ_{Zr}^{Au} (0% Zr) at 1500°C is known:

$$\Delta F_{rx} = +RT \ln \gamma_{Zr}^{Au}$$
$$= (4.575)\ (1773)\ (-3.824)$$
$$= -31.02\ \text{kcal}$$

and

$$\Delta F_{rx}\ (1063^\circ C) = (-31.02 + 1.01)\ \text{kcal.}$$
$$= -30.01\ \text{kcal}$$

At the melting point of Au, liquid and solid Au are in equilibrium and there is no difference in the free energies of Zr (in liquid Au, 0% Zr) and Zr (in solid Au, 0% Zr). Below the melting point of Au, the reaction becomes: Zr(solid,pure) → Zr(in solid Au, 0% Zr). The entropy associated with this reaction is close to zero and the ΔF_{rx} is relatively temperature insensitive to 1000°C. Therefore:

$$\Delta F_{rx}(1000^\circ C) \cong \Delta F_{rx}\ (1063^\circ C) = -30.01\ \text{kcal}$$

The γ_{Zr}^{Au} (0% Zr) at 1000°C can now be obtained:

$$\Delta F_{rx} = RT \ln \gamma_{Zr}^{Au}$$

$$\log_{10} \gamma_{Zr}^{Au} = \frac{-30.01 \times 10^3}{(4.575)(1273)} = -5.153$$

The γ_{Zr}^{Au} (7.1 at.% Zr) is obtained using regular solution theory at 1000°C knowing γ_{Zr}^{Au} (0% Zr) = $10^{-5.153}$.

$$\log_{10} \gamma_{Zr}^{Au} (7.1 \text{ at.\% Zr}) = \log_{10} \gamma_{Zr}^{Au} (0\% \text{ Zr}) + \frac{(3150)(0.929^2 - 1)}{(4.575)(1273)}$$

$$= -5.153 - 0.0741$$

$$= -5.227$$

The $\Delta F_f(ZrAu_4)$ can now be calculated; it can be expressed as $\Delta F_f^\circ (ZrAu_4) = + RT \ln (a_{Zr})(a_{Au})^4$. When the Au phase contains 7.1 at.% Zr, it is in equilibrium with $ZrAu_4$. Therefore:

$$a_{Zr}^{ZrAu_4} = a_{Zr}^{Au(7.1 \text{ at.\% Zr})} = \gamma_{Zr} x_{Zr}$$

$$= (10^{-5.227})(0.071) = (10^{-5.227})(10^{-1.149})$$

$$= 10^{-6.376}$$

Assuming Au to be an ideal solution to 7.1 at.% Zr, γ_{Au}^{Au} (7.1 at.% Zr) = 1 and:

$$a_{Au}^{ZrAu_4} = a_{Au}^{Au(7.1 \text{ at.\% Zr})} = x_{Au} = 0.929$$

$$= 10^{-0.0320}$$

Therefore:

$$\Delta F_f^\circ(ZrAu_4) = RT \ln a_{Zr} a_{Au}^4$$

$$= (4.575)(1273)(-6.376 - 4 \times 0.032)$$

$$= -37.88 \text{ kcal/mole}$$

Carrying out the same calculations for Au (13.0 at.+ Zr) gives a value of $\Delta F_f^\circ(ZrAu_4)$ = -41.36 kcal/mole. Therefore:

$$-37.9 \text{ kcal/mole} \geq \Delta F_f^\circ(ZrAu_4) \geq -41.4 \text{ kcal/mole}$$

APPENDIX C

Calculation of the Overall Atomic % Zr From the Volume Fraction of $ZrAu_4$ Phase Relative to Au (7.0 at.% Zr) Phase

40.0 ± 4.4 vol.% $ZrAu_4$ has been experimentally found in the sample. The $ZrAu_4$ phase has 20.0 at.% Zr present and the Au phase has 7.0 ± 1.0 at.% Zr present.

A. Theoretical Molar Volumes of Au and $ZrAu_4$

Au:

f.c.c. structure; 4 atoms per unit cell; $a_o = 4.0786$ Å [24]

$$\frac{\text{Volume}}{\text{Mole}} = \frac{(4.0786\ \text{Å})^3}{4\ \text{atoms}} \cdot \frac{6.023 \times 10^{23}\ \text{atoms/mole}}{(10^8\ \text{Å/cm})^3}$$

$$\bar{v}_{Au} = 10.22\ \text{cc/mole of Au}$$

$ZrAu_4$:

The crystal structure of $ZrAu_4$ is an A3 type (primitive hexagonal) superstructure. The principle orthohexagonal axes are: $a_o = 14.295$ Å $= 5 \times 2.859$ Å, $b_o = 5.006$ Å, $c_o = 4.845$ Å.[57] There are 20 atoms/unit cell. Orthohexagonal axes describe the hexagonal unit cell in an orthogonal coordinate system. Figure 11 illustrates the relation between the orthohexagonal axes and the other conventional hexagonal axes. H. M. Otte and A. G. Crocker go into more detail on the interrelations of hexagonal cell representations.[63]

$$\frac{\text{Volume}}{\text{G} \cdot \text{atom}} = \frac{(14.294)\ (5.006)\ (4.845)\ (\text{Å})^3}{20\ \text{atoms}} \cdot \frac{6.023 \times 10^{23}\ \text{atoms/g·atom}}{(10^8\ \text{Å/cm})^3}$$

$$= 10.44\ \text{cc/g·atom of } ZrAu_4$$

B. Highest At.% Zr Considering All Errors (44.4 vol.% $ZrAu_4$, 8.0 at.% Zr in Au)

$$\frac{\text{G} \cdot \text{atoms of } ZrAu_4}{\text{Moles of Au}} = \frac{44.4 \text{ cc of } ZrAu_4}{55.6 \text{ cc of Au}} \cdot \frac{10.22 \text{ cc/mole of Au}}{10.44 \text{ cc/g}\cdot\text{atom of } ZrAu_4}$$

$$= 0.7817 \text{ g}\cdot\text{atoms of } ZrAu_4\text{/mole of Au}$$

$$= 0.1563 \text{ mole of } ZrAu_4\text{/mole Au.}$$

Relative moles of Zr = 0.1563(1) + 0.08(1) = 0.2363 moles

Relative moles of Au = 0.1563(4) + 0.92(1) = 1.5452 moles

Relative total moles = 1.7815 moles

at.% Zr = (0.2363/1.7815) 100 = 13.26 at.%

C. Lowest At.% Zr Considering All Errors (35.6 vol.% $ZrAu_4$, 6.0 at.% in Au

$$\frac{\text{G} \cdot \text{atoms of } ZrAu_4}{\text{Moles of Au}} = \frac{35.6 \text{ cc of } ZrAu_4}{64.4 \text{ cc of Au}} \cdot \frac{10.22 \text{ cc/mole of Au}}{10.44 \text{ cc/g}\cdot\text{atom of } ZrAu_4}$$

$$= 0.5411 \text{ g}\cdot\text{atoms of } ZrAu_4\text{/mole of Au}$$

$$= 0.1082 \text{ moles } ZrAu_4\text{/mole of Au}$$

Relative moles of Zr = 0.1082(1) + 0.06(1) = 0.1682 moles

Relative moles of Au = 0.1082(4) + 0.94(1) = 1.3728 moles

Relative total moles = 1.5410 moles

at.% Zr = (0.1682/1.5410)100 = 10.91 at.%

D. Average At.% Zr

Therefore the average at.% Zr is 12.1±1.2 at.%.

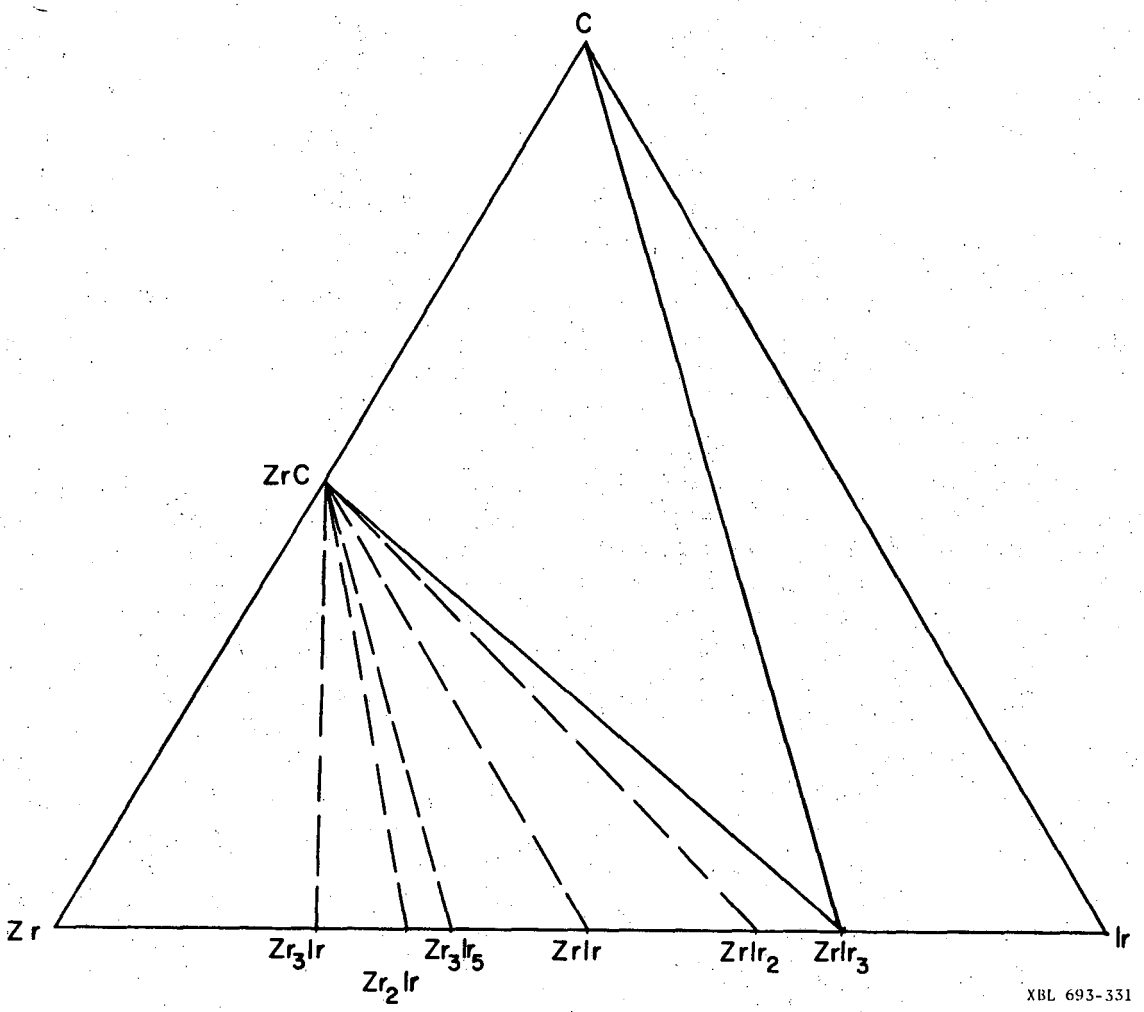

Fig. 1 The C-Zr-Ir ternary phase diagram. Although the diagram was determined at 1500°C, it is expected to exist as presented over a wide solidus temperature range. The solid joins indicate phases observed to exist in equilibrium. The dashed joins indicate phases expected to exist in equilibrium. The ZrM_2 ordered structure was also observed to exist in equilibrium with C and ZrC for the C-Zr-Rh, C-Zr-Pd (at 1380°C), and the C-Zr-Pt systems which are expected to have similar ternary phase diagrams.

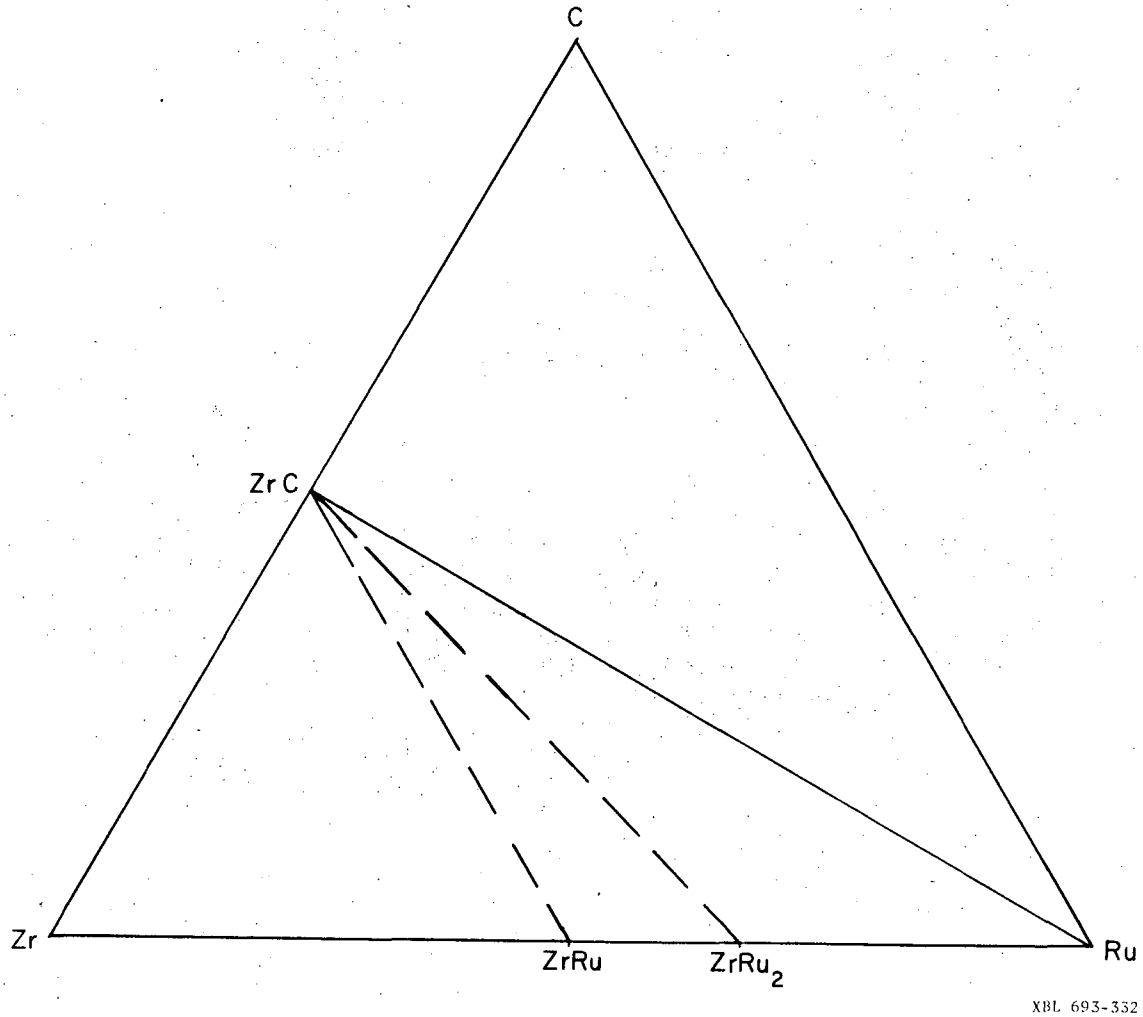

Fig. 2 The C-Zr-Ru ternary phase diagram. Although the diagram was determined at 1500°C, it is expected to exist as presented over a wide solidus temperature range. The solid joins indicate phases observed to exist in equilibrium. The dashed joins indicate phases expected to exist in equilibrium. Os was also observed to exist in equilibrium with C and ZrC; the C-Zr-Os system is expected to have a similar ternary phase diagram. From the liquid Ag and the liquid Au equilibrations with C and ZrC, the C-Zr-Ag and the C-Zr-Au ternary phase diagrams are expected to be similar at solidus temperatures.

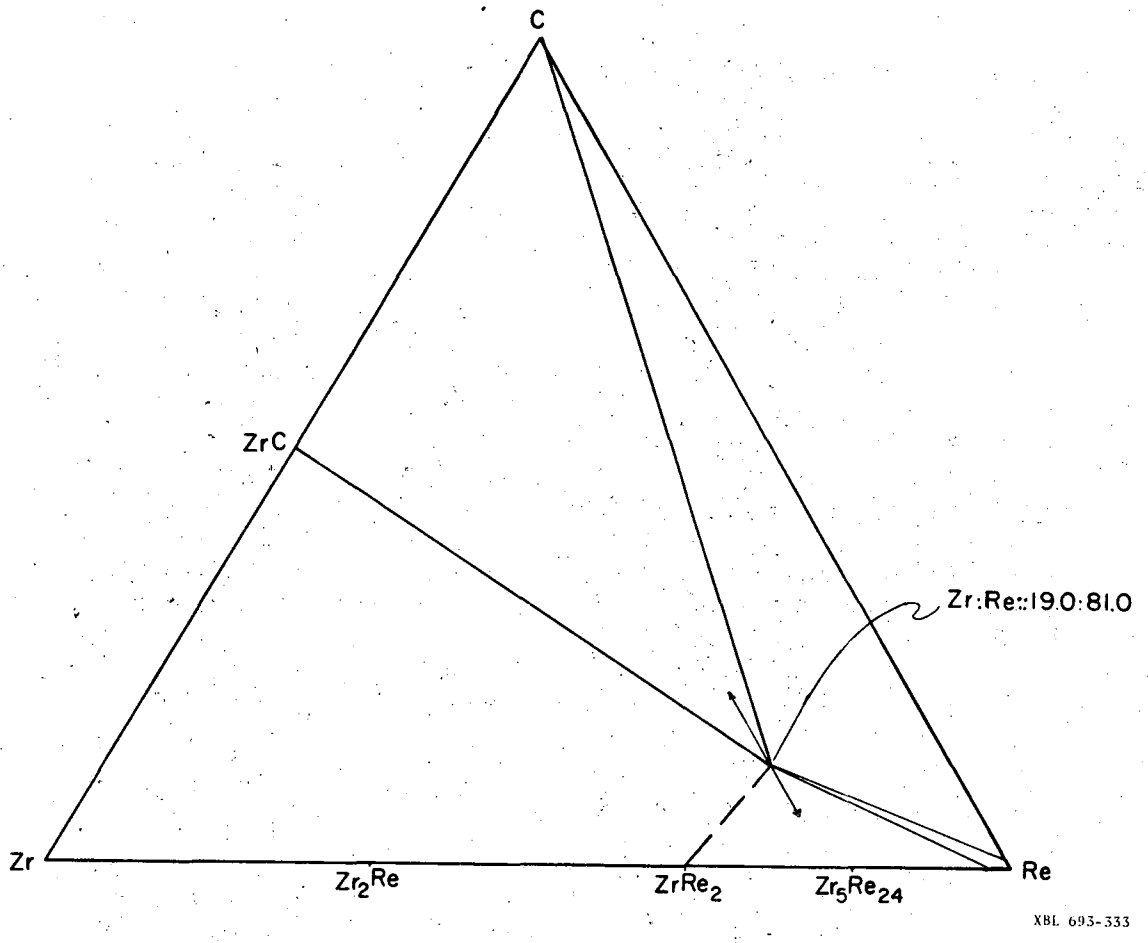

Fig. 3 The C-Zr-Re ternary phase diagram. Although the diagram was determined at 1500°C, it is expected to exist as presented over a wide solidus temperature range with the concentration of Zr in the Re phase varying with temperature. The solid joins indicate phases observed to exist in equilibrium. The dashed join indicates that the Re, the Zr_5Re_{24}, and the $ZrRe_2$ phases are expected to exist in equilibrium. Other joins between the ZrC phase and the $ZrRe_2$ and the Zr_2Re phases are not indicated by dashed joins because more ternary compounds are probable.

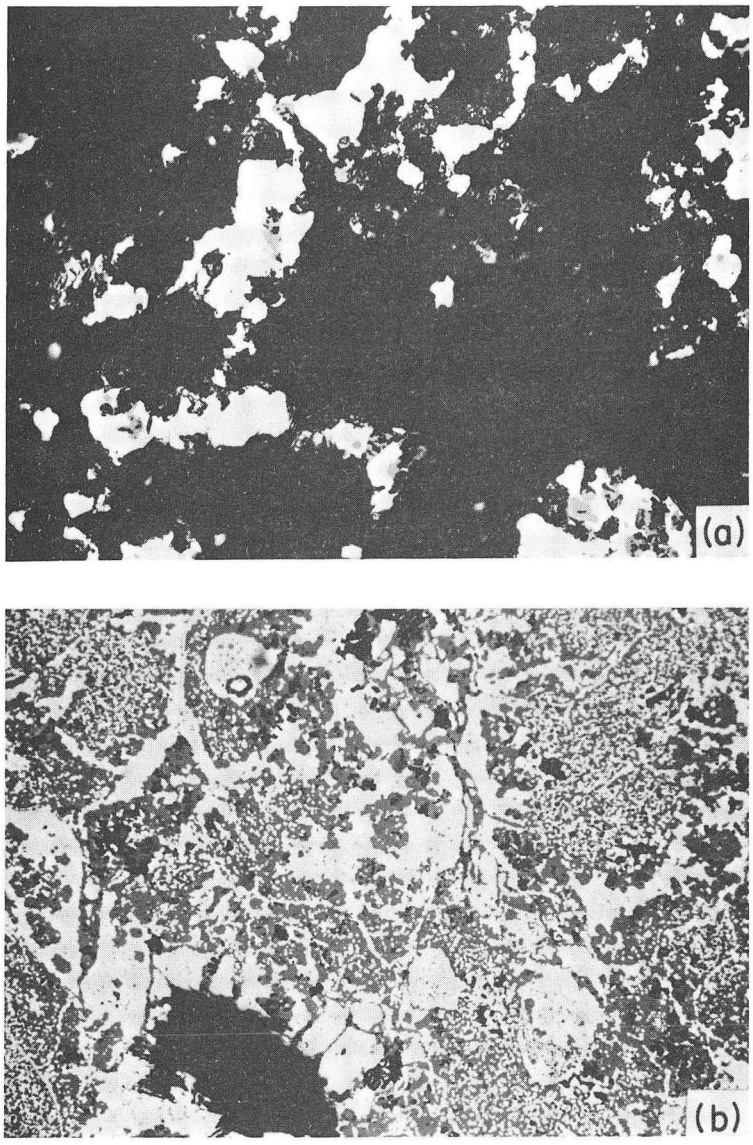

XBB 693-1777

Fig. 4 Equilibrations of the C-Zr-Ru ternary system (400×)
(a) The xC+ZrC+7Ru sample equilibrated for 130 hours at 1500°C.
(b) The 1.2C+ZrRu sample equilibrated for 88 hours at 1500°C.

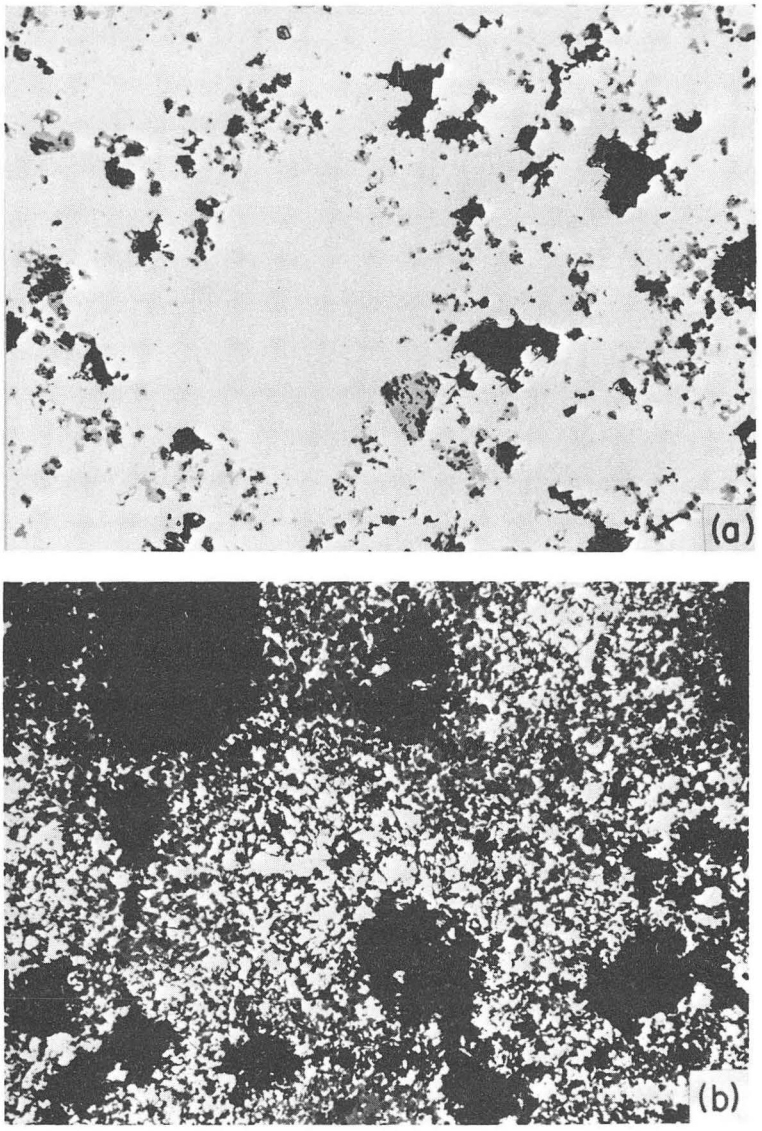

XBB 693-1778

Fig. 5 Equilibrations of the C-Zr-Os ternary system (400×)
(a) The xC+ZrC+7Os sample equilibrated for 120 hours at 1495°C.
(b) The 1.1C+$ZrOs_2$ sample equilibrated for 154 hours at 1490°C.

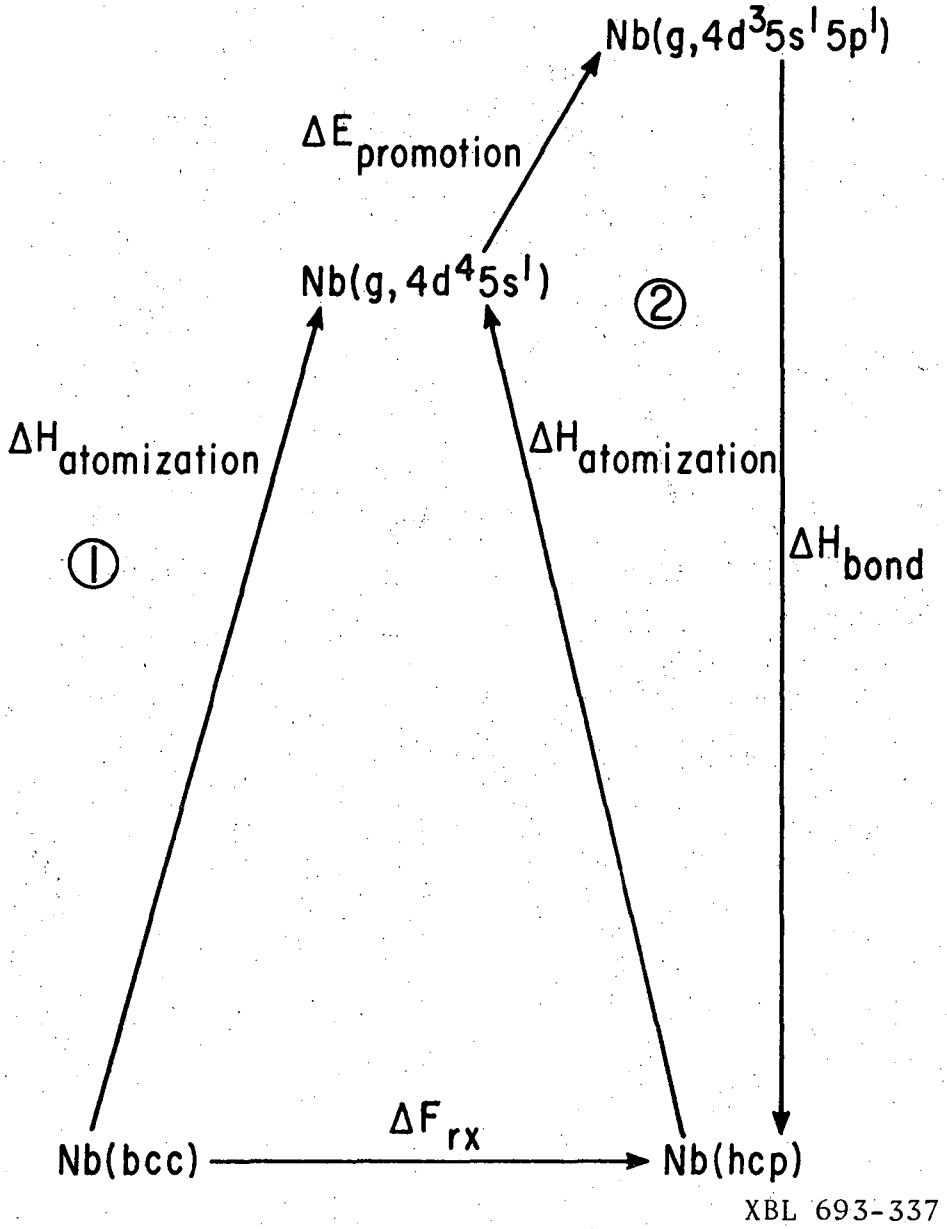

Fig. 6 The difference in free energy between bcc and hcp Nb(ΔF_{rx}) can be found indirectly by determining the values for the thermodynamic functions as indicated.

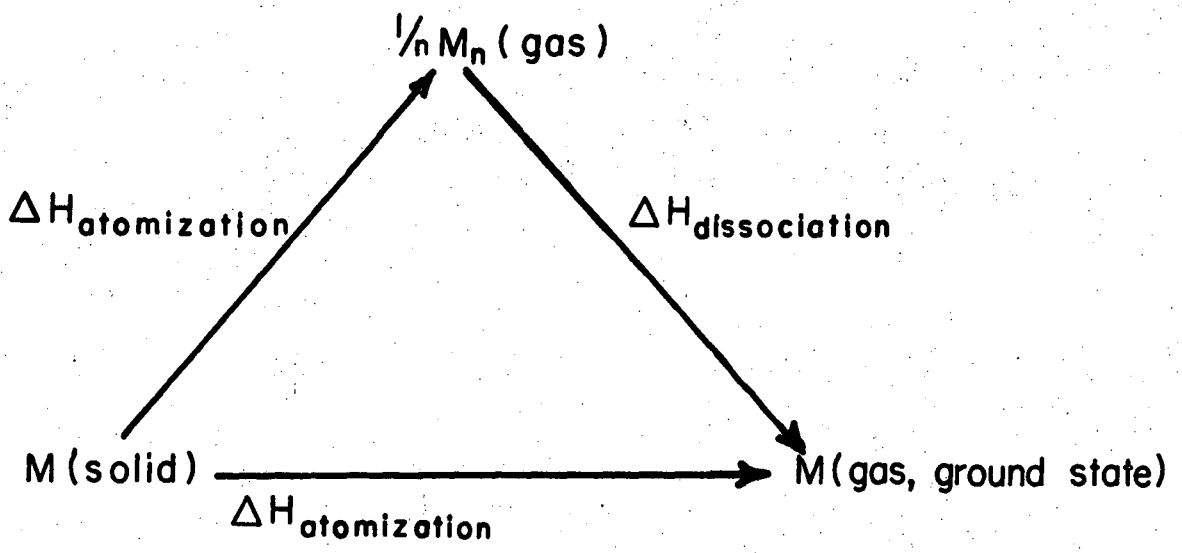

XBL 693-330

Fig. 7 If an element, M, does not vaporize to the monoatomic gas, $\Delta H_{atomization}$ is not equal to $\Delta H_{sublimation}$. $\Delta H_{atomization}$ can be found knowing the $\Delta H_{dissociation}$, however.

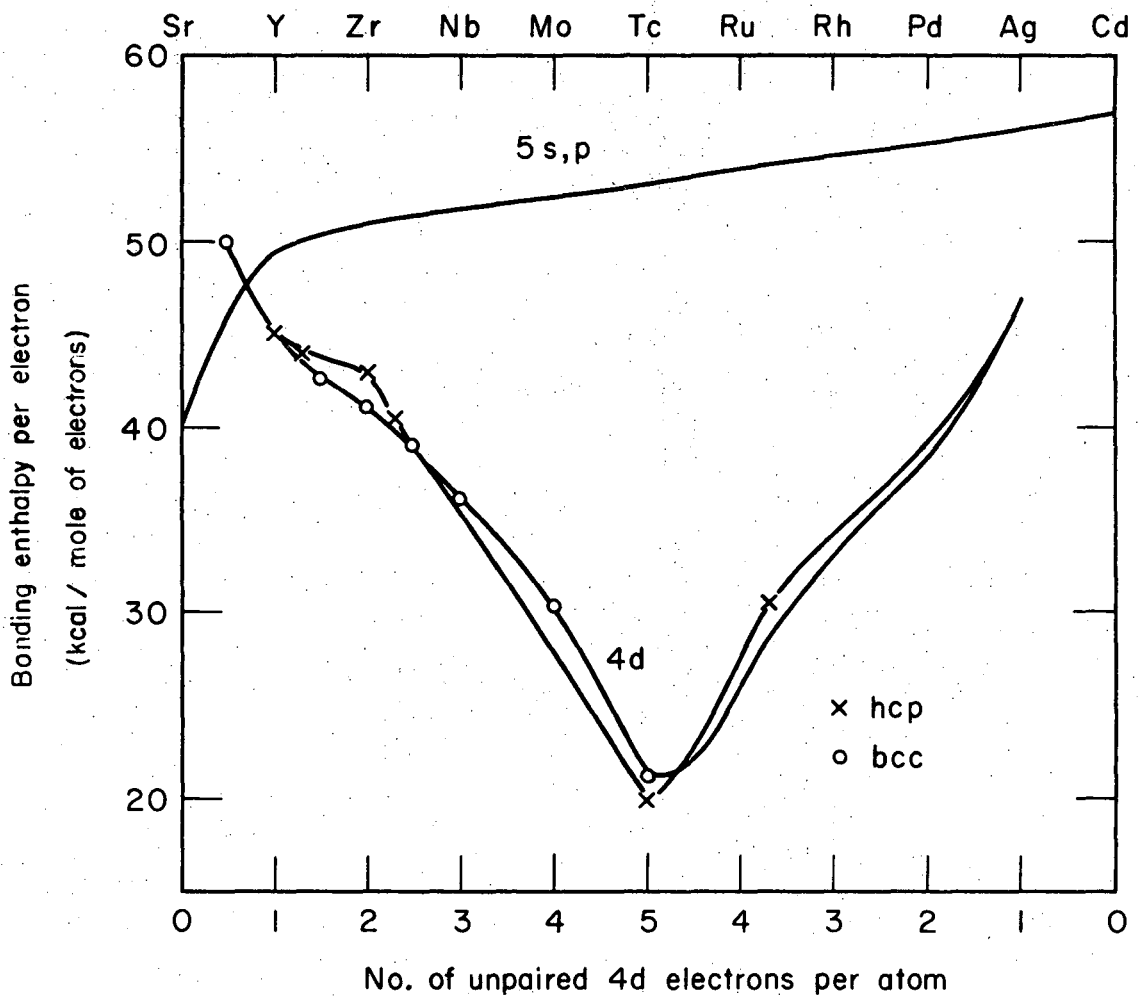

MUB-9307

Fig. 8 Bonding enthalpy per 5s or 5p electron versus atomic number and bonding enthalpy per 4d electron versus the number of unpaired 4d electrons per atom. For more accurate energy values than those which can be read off of the graph, see Table XII.

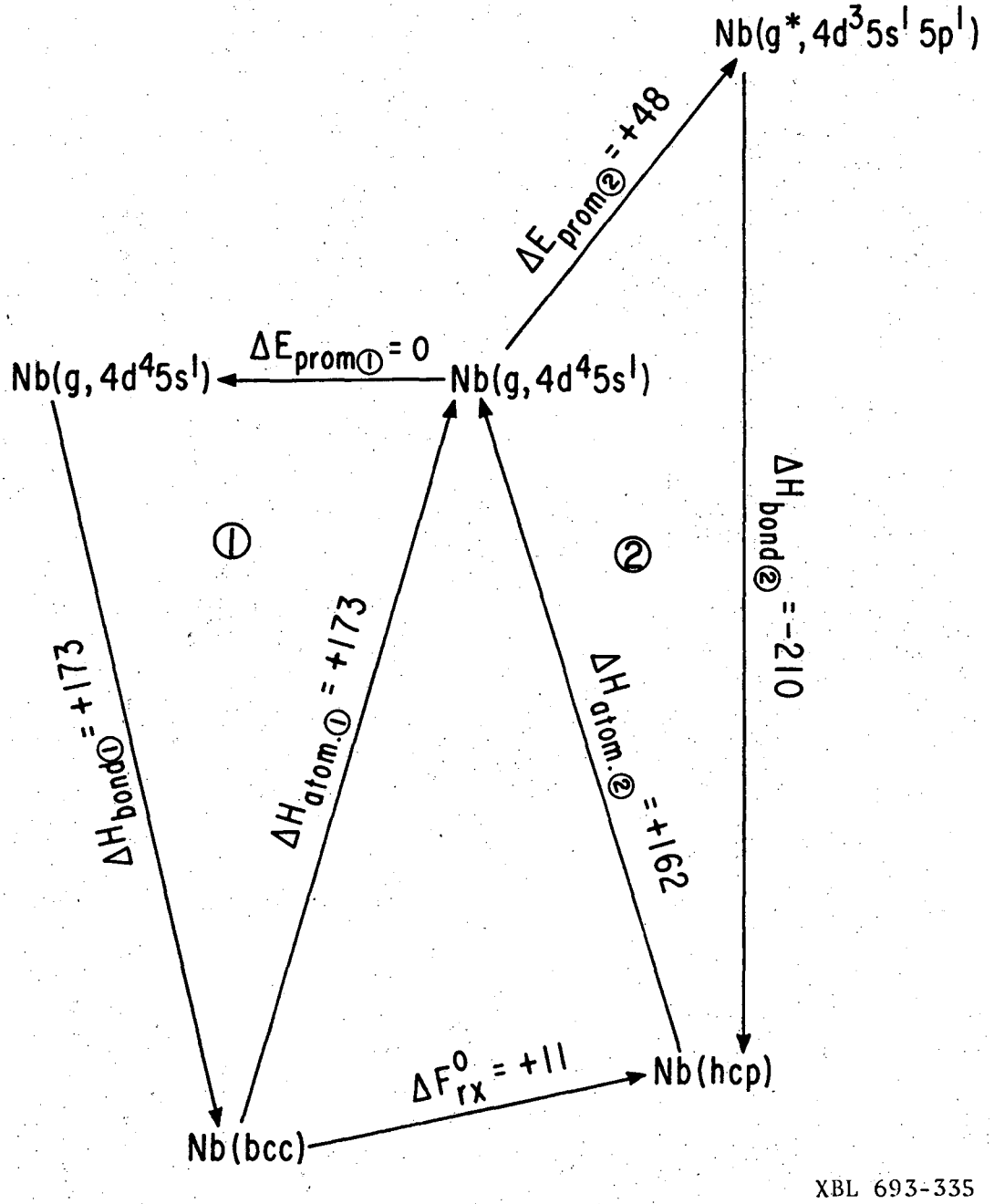

Fig. 9 Graphical representation of the energies considered in the Nb model using the integer representation of the Engel Correlation. All numerical values are given in units of kcal/mole.

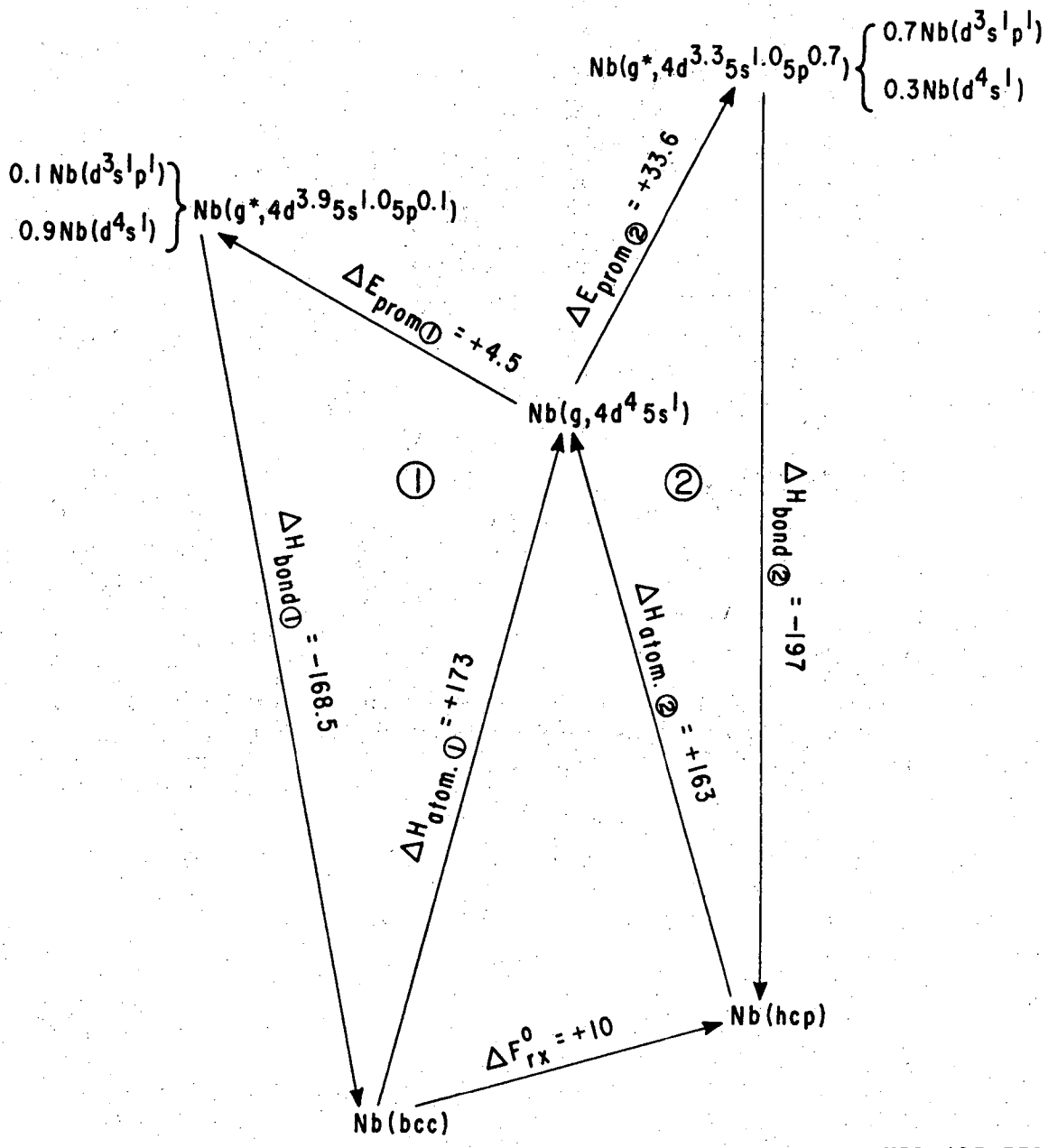

XBL 693-338

Fig. 10 Graphical representation of the energies considered in the Nb model using the nonintegral representation of the Engel Correlation. All numerical values are given in units of kcal/mole.

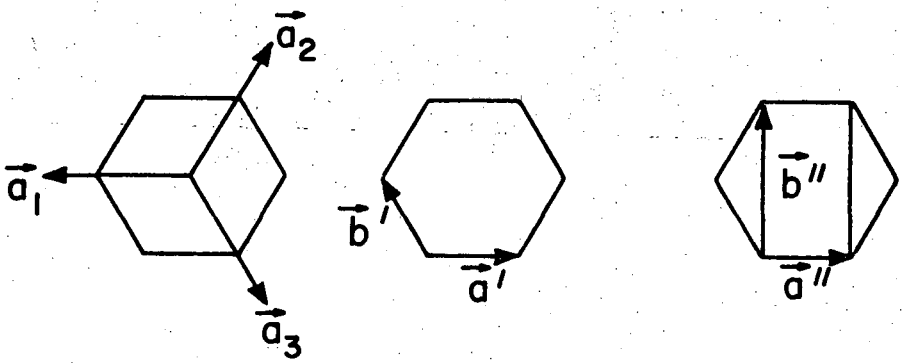

XBL 693-336

Fig. 11 The base of the hexagonal unit cell is expressed by the three vector notations commonly used: (1) 4-axis cell (a_1, a_2, a_3, c), (2) 3-axis cell (a', b', c') and (3) orthohexagonal cell (a", b", c"). All c axes are equal, irrespective of notation.

TABLE I. Electron microprobe analysis of the $Zr_{3.40}$ $Au_{96.60}$ standard.

a.

Atomic + Zr	Date	ST and STD for Zr within 3σ
3.47	8/19/68	yes (2.6σ)
3.48	12/ 5/68	no (3.5σ)
3.77	12/17/68	no (4.6σ)
2.96	1/10/69	yes (2.6σ)
2.96	1/11/69	no (5.5σ)
3.46	1/11/69	no (23σ)

b. Average Zr counts/20 secs. for 3.46 at.% Zr analysis

100% standard	30,012
Background for standard off of Nb	28
$Zr_{3.40}$ $Au_{96.60}$	450
Background for standard off of Au	52

TABLE II. Reactions of the C-Zr-Rh, C-Zr-Ir, C-Zr-Pt, C-Zr-Pd systems. The products were analyzed by x-ray diffraction. The "s", "m", and "w" refer to strong, medium, and weak intensities of the x-ray pattern. (1.0 bar = 0.987 atmosphere pressure.)

Reactants	Experimental Parameters	Phase Observed
ZrC + 1 Rh	1575°C 3 hours 490 bars vacuum	$\underset{s}{ZrRh_3}$ + $\underset{s}{ZrC}$ + $\underset{w}{C}$
ZrC + 1.78 Ir	1575°C 3 hours 490 bars vacuum	$\underset{s}{ZrIr_3}$ + $\underset{m}{ZrC}$ + $\underset{}{C}$ + $\underset{w}{Ir}$
ZrC + 2Pd	1380°C 3 hours 490 bars 600 torr Ar	$\underset{s}{ZrPd_3}$ + $\underset{m}{ZrC}$ + C
ZrC + 2Pt	1575°C 3 hours 490 bars vacuum	$\underset{s}{ZrPt_3}$ + $\underset{m}{ZrC}$ + $\underset{w}{C}$

TABLE III. Reactions of the C-Zr-Re, C-Zr-Ru, and C-Zr-Os systems. The products were analyzed with an electron microprobe analyzer; the obtained Zr concentrations are given. * This value was interpreted as interference from the ZrC phase and was not considered.

Reactants	Experimental Parameters	Phase Observed
$3.6C+1.5ZrC+1.0Zr_5Re_{24}$	1490±40°C 96 hours 350 bars 600 torr Ar	C+ZrC+Re(19.0 at.% Zr)
xC+ZrC+7Ru	1500±10°C 130 hours 600 torrs He	ZrC+C+Ru(0.74 at.% Zr)
1.2C+ZrRu	1500±30°C 88 hours 600 torr He	ZrC+C+Ru(0.76 at.% Zr)
xC+ZrC+7Os(0.62 at.%Zr)	1495±5°C 120 hours 600 torr He	ZrC+C+Os($\leq$ 0.059 at.% Zr)
$ZrOs_2$+1.1C	1490±10°C 154 hours 600 torr He	ZrC+C+Os(0.24 at.% Zr)*

Table IV. Reactions of the C-Zr-Ag and C-ZrAu systems.

Reactants	Experimental Parameters	Phases Observed
(a) Solid State Reactions		
ZrC+Ag	890°C 8 hours 490 bars 600 torr Ar	ZrC+Ag
1.2C+ZrAg	850°C±15°C 129½ hours 175 bars 600 torr Ar	ZrAg+C
ZrC+3Au	950°C 88 hours 175 bars 600 torr Ar	ZrC+3Au(0.51 at.% Zr)
C+$ZrAu_3$+$ZrAu_4$	925±15°C 110 hours 86 bars 600 torr Ar	$ZrAu_3$+$ZrAu_4$+C
(b) Liquid State Reactions		
C+ZrC+Ag	1410°C 15 hours 760 torr He	C+ZrC+Ag(<0.050 a/o Zr)
1.2C+ZrAg	1500°C 33 hours 760 torr He	C+ZrC+Ag(<0.050 a/o Zr)
C+ZrC+Au	1495°C 12¼ hours 760 torr He	C+ZrC+Au(0.87 a/o Zr)
C+$ZrAu_3$+$ZrAu_4$	1505°C 15½ hours 760 torr He	C+ZrC+Au (9.5±3.5 at.% Zr)

TABLE V. The activity coefficient of Zr(γ_{Zr}) is calculated from the three phase equilibria involving C and ZrC. Solution theory is used to determine γ_{Zr}(0% Zr) which is also expressed as the excess partial molar free energy of Zr in the limit of 0% Zr ($\bar{F}^{xs}_{Zr}$).

Atomic No. Element	at.% Zr	Corresponding $\log_{10} \gamma_{Zr}$	$\log_{10} \gamma_{Zr}$(0 at.%Zr)	$\bar{F}^{xs}_{Zr}$ (0 % Zr) (kcal/mole of Zr) calculated at 1500°C
44-Ru	0.75	-3.07	-3.07	-24.9
45-Rh	25.0	-4.59	$\leq$ -4.59	$\leq$ -37.2
46-Pd	25.0	-4.59	$\leq$ -4.59	$\leq$ -37.2
47-Ag	$\leq$ 0.50	$\geq$ -1.89	$\geq$ -1.89	$\geq$ -15.3
76-Os	$\leq$ 0.06	$\geq$ -1.96	$\geq$ -1.96	$\geq$ -15.9
77-Ir	25.0	-4.59	$\leq$ -4.59	$\leq$ -37.2
78-Pt	25.0	-4.59	$\leq$ -4.59	$\leq$ 37.2
79-Au	6.0 to 13.0	-3.97 to -4.31	-3.82 to -4.21	-31.0 $\geq \bar{F}^{xs}_{Zr} \geq$ -34.2

TABLE VI. The standard free energy of formation (ΔF_f°) of compounds of the Zr binary systems studied experimentally

Phase Information			Melting Point (°C); "p" implies peritectic melting; "c" implies congruent melting		ΔF_f° (kcal/g.atom) calculated at 298°K except when indicated
Stoichiometry	Structure: Pearson(a); Strukterbericht ; Type	References			
Zr_2Re	σ type phase a=10.12Å, c=5.42Å	26, 28	1900°C	p	———
$ZrRe_2$	hP12, C14, $MgZn_2$ a=5.269Å, c=8.626Å	26,28,44	2450°C	p	———
Zr_5Re_{24}	cI58, A12, α-Mn (?) a=9.693 to 9.698Å	26,28,44	2500°C	p	———
ZrRu	cP2, B2, CsCl a=3.253Å	29,44-46	2100°C 2130 ± 70°C*	c	$-9.5 \geq \Delta F_f^\circ \geq -21.7$ at 1500°C
$ZrRu_2$	hP12, C14, $MgZn_2$ a=5.141Å, c=8.509Å	25,44,45, 47,49	1960 ± 50°C	p	-13.6 ± 0.9 at 1500°C

TABLE VI. (continued)

Phase Information			Melting Point (°C); "p" implies peritectic melting; "c" implies congruent melting	ΔF_f° (kcal/g.atom) calculated at 298°K except when indicated
Stoichiometry	Structure: Pearson(a); Strukterbericht ; Type	References		
Zr_7Os_3	tetragonal, ϕHfRe type	3	———	$\geq$ -32.4
ZrOs	cP2, B2, CsCl a=3.263Å	28,44,46	———	$\geq$ -23.1
$ZrOs_2$	hP12, C14, $MgZn_2$ a=5.189Å, c=8.526Å	28,44, 47,48	2570 ± 80 c*	$\geq$ -15.4
Zr_2Rh	tI12, C16, Al_2Cu a=6.439$_7$Å, c=5.065$_8$Å	30,32 33	———	$\leq$ -5.1
ZrRh	cP2, B2, CsCl (above 380°C)[29]	29,30	———	$\leq$ -7.7
Zr_3Rh_5	NbRu type a=4.40Å, b=4.33Å, c=342Å	30	———	$\leq$ -9.6
$ZrRh_3$	cP4, L12, $AuCu_3$ a=3.927Å	28,30 44,49	———	$\leq$ -11.5

TABLE VI. (continued)

Phase Information			Melting Point (°C); "p" implies peritectic melting; "c" implies congruent melting	ΔF_f° (kcal/g.atom) calculated at 298°K except when indicated
Stoichiometry	Structure: Pearson(a); Strukterbericht ; Type	References		
Zr_3Ir	tP30, $D8_b$, σ or βU a=10.78Å, c=5.618Å	30,44	———	≤ -3.8
Zr_2Ir	tI12, C16, Al_2Cu	30,33	———	≤ -5.1
Zr_5Ir_3	Zr_5Ir_3 type	30	———	≤ -5.8
ZrIr	ZrIr type	30	———	≤ -7.7
$ZrIr_2$	cF24, C15, $MgCu_2$ a=7.359Å	30,44 47,50	———	≤ -10.3
$ZrIr_3$	cP4, $L1_2$, $AuCu_3$ a=3.943Å	44,49	2125 ± 135°C *	≤ -11.5
Zr_2Pd	tI6, $C11_b$, $MoSi_2$ a=3.306Å, c=10.894Å	28,35,36 44,51,52,53	1085°C c	≤ -5.1

TABLE VI. (continued)

Phase Information			Melting Point (°C); "p" implies peritectic melting; "c" implies congruent melting		ΔF_f° (kcal/g.atom) calculated at 298°K except when indicated
Stoichiometry	Structure: Pearson(a); Strukterbericht ; Type	References			
ZrPd	TiNi type (below M_f)[29]	29, 35 36	> 1600°C	c	$\leq$ -7.7
$Zr_{44}Pd_{56}$	?	3,28,35	———		$\leq$ -8.6
$ZrPd_2$	tI6, $C11_b$, $MoSi_2$ a=3.40$_7$Å, c=8.59$_7$Å	35,36 44,53	———		$\leq$ -10.2
$ZrPd_3$	hP16, DO_{24}, $TiNi_3$ a=5.612Å, c=9.235Å	35,36 44,49	———		$\leq$ -11.5
Zr_4Pt	tetragonal, ϕHfRe type	3	———		$\leq$ -3.1
Zr_2Pt	Zr_5Ir_3 type	30,33	1725°C	p	$\leq$ -5.1
ZrPt	oC8, B_f, ζ-BCr a=3.409Å, b=10.315Å, c=4.277Å	30,44 54	2100°C		$\leq$ -7.7

TABLE VI. (continued)

Phase Information			Melting Point (°C); "p" implies peritectic melting; "c" implies congruent melting		ΔF_f° (kcal/g.atom) calculated at 298°K except when indicated
Stoichiometry	Structure: Pearson(a); Strukterbericht ; Type	References			
$ZrPt_{+1}$	cP2, B2, CsCl a=3.31Å	30,44	2100°C		$\leq$ -7.7
Zr_4Pt_5	?	30	———		$\leq$ -8.5
Zr_2Pt_3-	?	30	———		$\leq$ -9.2
$ZrPt_3$	hP16, DO_{24}, $TiNi_3$ a=5.645Å, c=9.235Å	28,30 44,58	> 2120°C	c	$\leq$ -11.5
Zr_2Ag	tI6, $C11_b$, $MoSi_2$ a=3.2464Å, c=12.004Å	28,38,44 51,52			$\geq$ -30.8
ZrAg	tP4, B11, γ-CuTi a=3.468Å, c=6.603Å	28,38 44,55	1160°C	c	$\geq$ -23.1
Zr_3Au	cP8, A15, β-W a=5.4824Å	35,44 56	———		-2.37 $\geq \Delta F_f^\circ \geq$ -31.0 at 1000°C

TABLE VI. (continued)

Phase Information			Melting Point (°C); "p" implies peritectic melting; "c" implies congruent melting		ΔF_f° (kcal/g.atom) calculated at 298°K except when indicated
Stoichiometry	Structure: Pearson(a); Strukterbericht ; Type	References			
Zr_2Au	tI6, $C11_b$, $MoSi_2$ $a=3.27_2$Å, c=11.50Å	35,44 51,52	———		$-3.16 \geq \Delta F_f^\circ \geq -27.6$ at 1000°C
Zr_7Au_{10}	tI $a=6.69_6$Å, $c=13.29_2$Å	35,44	———		$-5.57 \geq \Delta F_f^\circ \geq -17.0$ at 1000°C
$ZrAu_2$	tI6, $C11_b$, $MoSi_2$ $a=3.53_2$Å, $c=8.71_8$Å	34,35,44	———		$-6.31 \geq \Delta F_f^\circ \geq -13.8$ at 1000°C
$ZrAu_3$	orthorhombic, β-Cu_3Ti $a=6.06_2$Å, $b=4.86_5$Å, $c=4.78_5$Å	35,44,57	1560°C	c	$-7.10 \geq \Delta F_f^\circ \geq -10.3$ at 1000°C
$ZrAu_4$	orthorhombic subcell, D_{2h}^{16} (Pnma)-Pbnm orthogonal axes: $5a=5(2.85_8)=14.29_4$Å b=5.006Å, $c=4.84_5$Å 20 atoms/unit cell	35,44,57	~1065°C		$-7.58 \geq \Delta F_f^\circ \geq -8.27$ at 1000°C

TABLE VI. (continued)

(a) Pearson nomenclature was used because of its condensation of much directly readable information. A brief description from Ref. 44 is in order. The first small letter denotes: a = triclinic (anorthic); m = monoclinic; o = orthorhombic, t = tetragonal, h = hexagonal, and c = cubic. The capital letters imply: P = primitive; C = one-face-centered; F = all-face-centered; I = body-centered, R = rhomdehedral. The number following gives the number of atoms in the crystallographic cell.

* These melting points were experimentally observed; the others are reported in the literature.

TABLE VII. Boride reactions reported by J. M. Criscione et al.[20]

Reactants	Experimental Parameters	Phases Observed	Minimum Reaction Temperatures (°C)
ZrB_2 + 4.75Rh	1430°C 1/2 hour	$ZrRh_3$ + ?	1195 ± 5
ZrB_2 + 4.75Ir	1430°C 1/2 hour	$ZrIr_3$ + ?	1220 ± 5
HfB_2 + 4.75Rh	1430°C 1/2 hour	$HfRh_3$ + ?	1165 ± 5
HfB_2 + 4.75Ir	1430°C 1/2 hour	$HfIr_3$ + ?	1235 ± 5

TABLE VIII HfC and ThC_2 reactions reportedly J. M. Criscione et al.[20] and N. H. Kirkorian et al.[39]

Reactants	Experimental Parameters	Phase Observed
HfC+3Rh	> 1000°C	$HfRh_3$
HfC+3Ir	2050°C 1/2 hour	$HfIr_3$
ThC_2+2Ir	not given	$ThIr_2$
ThC_2+2Rh	1900°C(melt) vacuum	?
ThC+3Au	850°C 114 hours 4×10^{-6} Torr	$ThAu_3$(?)

TABLE IX. Reactions of NbC and TaC, reportedly by Larry Kaufman et al.[40] and Peter Riesenfeldt.[41]

NbC+3Re	1200°C	no change
	1700°C	$NbRe_{3\pm x}$ (α Mn Structure) ? + C
NbC+Ru	1200°C	no change
NbC+3Ir	1200°C	no change
	1500°C	$NbIr_3$+C
NbC+3Pt	1200°C and 1500°C	$NbPt_3$ (α and β) + C
TaC+3Pt	1400°C and 1600°C, ½ hour, 600 bars	$TaPt_3$+C

TABLE X. Reactions of UC, and ThC, and UN reported by N. H. Krikorian.[39]

$2UC + Ir \xrightarrow[\sim 1700°C]{} U_2IrC_2$	
$2UC + Rh \xrightarrow[\sim 1700°C]{} U_2RhC_2$	
$UC + 3Ir \xrightarrow[1400°C \text{ and } 1700°C]{} UIr_3 + C$	
$UC + 3Rh \xrightarrow[1400°C \text{ and } 1700°C]{} URh_3 + C$	
$UC + 3Au(s) \xrightarrow[\substack{< 950°C \\ 17 \text{ hours} \\ 10^{-6} \text{ torr}}]{} UAu_3 + C$	
$UC + 3Au(l) \xrightarrow[\substack{> 1100°C \\ 18 \text{ hours} \\ 10^{-6} \text{ torr}}]{} UAu_3 + C$	
$2UN + 6Au \xrightarrow[\substack{860°C \\ \text{vac} = 4\times10^{-6} \\ 47 \text{ hours}}]{} 2UAu_3 + N_2$	
$UN + Au \xrightarrow[\substack{860°C \\ 93h \\ 0.75 \text{ atm } N_2}]{} U_2N_3 + Au$	

TABLE XI. The standard free energy of formation (ΔE_f°) calculated from the reactions reported by other authors

Compound	ΔF_f° (Kcal/g.atom) calculated at 298°K	ΔF_f° was obtained by comparison with:	Reference
$ZrRh_3$	$\leq$ -11.5	ZrC	20*
	$\leq$ -19.2 ?	ZrB_2	20
$ZrIr_3$	$\leq$ -11.5	ZrC	20*
	$\leq$ -19.2 ?	ZrB_2	20
$HfRh_3$	$\leq$ -12.7	HfC	20
	$\leq$ -19.4 ?	HfB_2	20
$HfIr_3$	$\leq$ -1.27	HfC	20
	$\leq$ -19.4 ?	HfB_2	20
$ThIr_2$	$\leq$ -8	ThC_2	20
$ThRh_2$	$\leq$ -8 ?	ThC_2	20
$ThAu_3$	$\leq$ -6 ?	ThC	39
$NbPt_3$	$\leq$ -8.4	NbC	40
$NbIr_3$	$\leq$ -8.4	NbC	40
$NbRe_{3\pm x}$	$\leq$ -8.4 ?	NbC	40
$TaPt_3$	$\leq$ 8.8	TaC	41
UIr_3	$\leq$ -5.9	UC	39
URh_3	$\leq$ -5.9	UC	39
U_2IrC_2	$\leq$ -9.4	UC	39
U_2RhC_2	$\leq$ -9.4	UC	39
UAu_3	$-5.9 \geq \Delta F_f^\circ \geq -12.5$	UC and UN	39
$CePt_2$	$\Delta H_f^\circ \sim -55$	CeS	64

* These limits agree with the experimental observations determined in this research.

TABLE XII Bonding enthapies and number of bonding d electrons for the elements of period 4: (a); of Period 5: (b); and of Period 6 : (c). $E_p \equiv$ bonding enthalpy per s or p electron; $E_d \equiv$ bonding enthalpy per d electron; $N_d \equiv$ number of bonding d electrons per atom. For $n_d < 5$, $N_d = n_d$; for $n_d > 5$, $N_d = 10 - n_d$.

(a)

Elements with 3d e⁻'s		Ca	Sc	Ti	V	Cr	Mn	Fe	Co	Ni	Cu	Zn
	E_p	42.5	51.0	52.5	54.0	55.0	56.0	57.0	58.0	60.0	61.0	62.0
bcc	N_d	0.5	1.5	2.5	3.5	4.5	4.5	3.5	2.5	1.5		
	E_d	58.0	34.5	25.8	19.5	10.8	7.7	14.7	21.0	30.0		
hcp	N_d	0.3	1.0	2.0	3.0	4.0	5	3.7	2.7	2.0	0.7	
	E_d	56.0	33.5	26.0	19.0	12.0	1.7	12.3	19.5	25.5	45.0	

(b)

Elements with 4d e⁻'s		Sr	Y	Zr	Nb	Mo	Tc	Ru	Rh	Pd	Ag	Cd
	E_p	40.0	49.5	51.0	$51^{2/3}$	$52^{1/3}$	53.0	54.0	$54^{2/3}$	$55^{1/3}$	56.0	57.0
bcc	N_d	0.5	1.5	2.5	4.0	5.0	4.5	3.0	2.0	1.0		
	E_d	50.0	42.5	38.5	30.1	21.0	22.0	32.3	38.0	47.0		
hcp	N_d	0.3	1.3	2.3	3.3	4.3	5.0	3.7	2.7	1.7		
	E_d	52.0	44.0	40.5	33.0	25.4	19.8	30.2	35.5	41.0		

(c)

Elements with 5d electrons		Lu	Hf	Ta	W	Re	Os	Ir	Pt	Au	Hg
	E_p	50.5	52	53	$53^{2/3}$	$54^{1/3}$	55	56	57	59	61.5
bcc	n_d		2.5	3.5	5.0	4.5	3.5	2.5	1.5		
	E_d		46.0	41.8	31.4	32.5	38.5	45.0	54.0		
hcp	n_d		2.3	41.5	4.0	5.0	4.0	3.0	2.0	0.7	
	E_d		46.5	3.0	34.0	26.5	36.3	40.5	50.5	57.0	

TABLE XIII

Metallic electron to atom ratio limits

(a) From Leo Brewer

structure	No. of s and p e^-'s Bonding per Atom (n_p)	% p-character (ref. b)
b.c.c.	1 - 1.5	0 - 33
h.c.p.	1.7 - 2.1	41 - 52
c.c.p. (f.c.c.)	2.25- 3.0	60 - 67

(b) From Niels Engel (g)

structure	No.of s and p e^-'s bonding per Atom (n_p)
b.c.c.	1.0 - 1.7
h.c.p.	1.9 - 2.25
c.c.p.	2.25 - 3.$^+$

ACKNOWLEDGEMENTS

I wish to acknowledge the assistance offered by the people associated with the Inorganic Materials Research Division of the Lawrence Radiation Laboratory, the financial support provided by the Atomic Energy Commission, the patience and understanding given by my wife and the kind and inspirational guidance offered by my research director, Leo Brewer.

REFERENCES

1. L. Brewer, Viewpoint of Stability of Metallic Structure, in Battelle Geneva Colloquim on Phase Stability in Metals and Alloys, P. Rudman, J. Stringer, and R. L. Jaffe, eds., (McGraw-Hill Book Company, New York, 1967). Also available as UCRL-16250.

2. L. Brewer, Bonding and Structure of Transition Metals, Science 161, [3837], 115-161, July 12, 1968.

3. L. Brewer, Prediction of High Temperature Metallic Phase Diagrams, in High Strength Materials, V. F. Zackay, ed. (John Wiley and Sons, New York, 1965). An earlier draft was issued as UCRL-10701, Rev. 2, August 1964.

4. L. Brewer, A Most Striking Confirmation of the Engel Metallic Correlation, Acta Met. 15, 553-556 (1967).

5. L. Brewer, Thermodynamic Stability and Bond Character in Relation to Electronic Structure and Crystal Structure, in Electronic Structure and Alloy Chemistry of the Transition Elements, Paul A. Beck, ed., (Interscience Publishers, New York, 1963).

6. N. N. Engel, Some New Viewpoints on the Metallic Bond, Ingenioren, M101 (1939), M1 (1940); Haandlogi Metalare: Selskabet for Metalorskning, Copenhagen, 1945; Kem. Maanedsbled, No. 5,6,8,9 and 10 (1940), (in Danish). A mimeographed manuscript in English was circulated in this country in the late forties and early fifties. A brief summary is given in Powder Metallurgy Bulletin, 7, 8 (1954).

7. N. N. Engel, Copper, Copper Alloys and the Electron Concentration Concept, Acta Met. 15, 557-563 (1966).

8. W. Hume-Rothery, A Note on the Engel-Brewer Theory of Metallic Structures, Acta Met. 13, 1039-1042 (1965).

9. W. Hume-Rothery, The Engel-Brewer Theories of Metals and Alloys, in Progress in Materials Science, 13 (Pergamon Press, Oxford, 1968), pp. 229-265.

10. R. Hultgren, R. L. Orr, and K. K. Kelley, Supplement to Selected Values of Thermodynamic Properties of Metals and Alloys, HfB_2: May 1968, ZrB_2: May 1967, HfC; Feb. 1966, NbC: Dec. 1965, TaC: Dec. 1965, ThC and ThC_2: Dec. 1966, UC: Aug. 1967, ZrC: Oct. 1966.

11. M. R. Pickus, unpublished work.

12. S. Z. Fraser, R. W. Fitzgerald, and A. M. Reid, Computer Programs EMX and EMX 2 for Electron Microprobe Data Processing, paper presented at First National Conference on Electron Microanalysis, College Park, Maryland, 1966.

13. L. S. Birks, Electron Probe Microanalysis, (Interscience Publishers, New York, 1963), p. 125.

14. H. A. Elion, Instrument and Chemical Analysis Aspects of Electron Microanalysis and Macroanalysis, Vol. 5 in Analytical Chemistry, Series IX of Progress in Nuclear Energy, (Pergamon Press, Ltd., London, 1966).

15. J. W. Colby, MAGIC - A Computer Program for Quantitative Electron Microprobe Analysis, Bell Telephone Laboratories, Inc., unpublished.

16. R. D. Giauque, A Radioisotope Source-Target Assembly for X-Ray Spectrometry, Analytical Chem. 40, [13], 1075-1077 (1968).

17. H. S. de Ben, Estimation of Detection Limits in Electron Probe Microanalysis, from Electron Probe Analysis Society of America, Third National Conference of Electron Microprobe Analysis, July 31 to August 2, 1968.

18. E. Nembach, Superconducting Transition Temperatures of Various

Lead-Base Alloys, J. Phys. Chem. of Solids, 29, 1205-1211 (1968).

19. L. S. Darken and R. W. Gurry, Physical Chemistry of Metals, (McGraw-Hill Book Company, New York, 1953).

20. J. M. Criscione, R. A. Mercuri, E. P. Schram, A. W. Smith, and H. F. Volk, High Temperature Protective Coatings for Graphite, Air Force Materials Laboratory, Wright Patterson Air Force Base, Ohio, Report No. ML-TDR-64-173, Part II, October 1964.

21. Gerald Stowe, Study of the Zr-Pt System by H_2 Reduction, report for Chemistry course 106, University of California, Berkeley, June 2, 1965.

22. W. Worrell, personal communication, February 1969.

23. W. Rostoker and J. R. Dvorak, Interpretation of Metallographic Structures, (Academic Press, New York, 1965), p. 195-219.

24. X-Ray Powder Data File, ASTM Special Technical Publication 48-J, J. V. Smith, ed., (American Society for Testing Materials, Philadelphia, Pa., 1960), Re: No, 5-0702, 1953; Au:No. 40784, 1950.

25. M. Hansen, Constitution of Binary Alloys, (McGraw Hill Book Company, New York, 1958).

26. E. M. Savitskii, M. A. Tylkina, Some Physical Properties of Rhenium and its Alloys, in Rhenium, B. W. Gonser, ed., a series of papers presented at the Sympoisum on Rhenium of the electrothermics and Metallurgy Division of the Electrochemical Society, May 3 and 4, 1960.

27. D. E. Williams, LCR-2, A Fortran Lattice Constant Refinement Program, Ames Laboratory at Iowa State University of Science and Technology, Report No. IS-1052, November 1964.

28. R. P. Elliott, Constitution of Binary Alloys, First Supplement, (McGraw Hill Book Company, New York, 1965).

29. F. E. Wang, J. Appl. Phys. 38, 822-824 (1967).

30. A. Raman and K. Schubert, Z. Metal 55, 704-710 (1964).

31. C. J. Raub and C. A. Anderson, Z. fur Physik, 175, 105-114 (1963).

32. S. T. Zegler, J. Phys. Chem. Solids, 26, 1347-1349 (1965).

33. M. V. Nevitt, J. W. Downey and R. A. Morris, Trans. AIME, 218, 1019-1023 (1960).

34. M. V. Nevitt, Alloy Chemistry of Transition Elements, in Electronic Structure and Alloy Chemistry of the Transition Elements, Paul A. Beck, ed., (Interscience Publishers, New York, 1963), p. 134.

35. E. Stolz and K. Schubert, Z. Metall. 53, 433-444 (1962).

36. K. Anderko, Z. Metall. 50, 681-685 (1959).

37. N. Karlsson, Acta Chem. Scand. 6, 1424 (1952).

38. J. O. Betterton, Jr., and D. S. Easton, Trans. AIME, 212, 470-5 (1958).

39. N. H. Krikorian, T. C. Wallace, M. C. Krupka, and C. L. Radosevich, The Reaction of Some Noble and Transition Metals with Refractory Carbides, J. Nuc. Matl. 21, 236-8 (1967).

40. L. Kaufman, personal communication with Leo Brewer. August 18, 1966.

41. Peter Riesenfeldt, report for the University of Calif, Chemistry Course, 1966.

42. V. W. Bronger and W. Klemm, Description of the Alloys of Pt with Non-Precious Metals, Z. fur Anor. Chem. 319, 58-81 (1962); in German. Note: Reactions 1 and 2, pg. 59 are not balanced:

1. $Al_2O_3 \rightarrow 2Al(\ell) + 3/2\ O_2$

From the U. S. Bureau of Mines, Bulletin 542, 1954: $\Delta F_f\ (Al_2O_3)$ = -285.3 kcal/mole at 1500°K ≃ 1200°C. Therefore, $\Delta F_{rx\ 1}$ = + 285.3 kcal and the equilibrium $P_{O_2} = 10^{-28}$ atm.

2. $Al_2O_3 + 6Pt \rightarrow 2Pt_3Al + 3/2\ O_2$

$\Delta F_{rx\ 2} = 2\Delta F^{\circ}_f (Pt_3Al) - \Delta F^{\circ}_f(Al_2O_3)$.

The assumed value of $\Delta F_f(Pt_3Al)$ is given as -30 kcal/mole. $\Delta F_{rx\ 2} = 2(-30)-(-285) = +225$ kcal and at equilibrium $P_{O_2} = 10^{-22}$ atm. The above arithmetic errors do not change the sense of the point being discussed in this paragraph.

43. U. S. Bureau of Mines Bulletin 542, 1954.

44. W. B. Pearson, Handbook of Lattice Spacings and Structures of Metals Vol. 2, (Pergamon Press Inc., New York), pp. 1-4; 106 (Zr-Ag), 160 (Zr-Au), 300 (Zr-Ir), 349 (Zr-Os), 359 (Zr-Pd), 365 (Zr-Pt), 372 (Zr-Rh), 374 (Zr-Ru), 537 (Zr-Ag)(1967).

45. E. Raub and E. Roschel, Z. Metall. 54, 455-462 (1963).

46. A. E. Dwight, Trans. AIME, 215, 283-286 (1959).

47. H. J. Wallbaum, Naturwiss. 30, 149 (1952).

48. A. E. Dwight, ANL 6330 (Annual Report), 155-158 (1960).

49. A. E. Dwight and P. A. Beck, Trans. AIME, 215, 976-979 (1959).

50. A. E. Dwight, Trans. ASM 53, 479-500 (1961).

51. M. V. Nevitt, ANL 6330 (Annual Report), 164-165 (1960).

52. M. V. Nevitt and J. W. Downey, Trans. AIME 224, 195 (1962).

53. K. Schubert, S. Bhan, W. Burkhardt, R. Gohle, H. G. Meissner, M. Potzschke, and E. Stolz, Naturwiss. 47, 303 (1960).

54. A. E. Dwight, R. A. Conner, Jr. and J. W. Downey, Acta. Cryst. 18, 835-839 (1965).

55. E. Raub and M. Engel, Z. Metall. 39, 172-177 (1948).

56. M. V. Nevitt, Trans. AIME, 224, 350-355 (1958).

57. K. Schubert, M. Bal, S. Bhan, H. Breimer, P. Esslinger, and E. Stolz, Naturwiss. 46, 647-648 (1959).

58. H. J. Wallbaum, Naturwiss. 31, 91-92 (1943).

59. L. Brewer and B. Olinger, personal communication, December, 1968.

60. L. Brewer, personal communication.

61. R. G. Lye, Band Structure and Bonding in Titanium Carbide, in Atomic and Electronic Structure of Metals, Gilman and Teller, eds. ASM, 1967.

62. L. Kaufman and H. Bernstein, Development and Application of Methods for Predicting the Temperature-Composition Stability of Refractory Compounds, Air Force Materials Laboratory, Wright Patterson AFB, Ohio, AFML-TR-67-108, 172 pp. April 1967 and AFML-TR-67-397, 90 pp. December 1967.

63. H. M. Otte and A. G. Crocker, Crystallographic Formulae for Hexagonal Lattices, Phys. Stat. Sol. 9, 441-450 (1965).

64. E. D. Eastman, Leo Brewer, LeRoy A. Bromley, Paul W. Gilles, and Norman L. Lofgren, "Preparation and Tests of Refractory Sulfide Crucilbes", The Journal of the American Ceramic Society, 34, 4, 128-134, 1951.

65. M. W. Evans, The Heats of Formation of CeS, Ce_3S_4, and Ce_2S_3 at 25° in the book The Chemistry and Metallurgy of Miscellaneous Materials Thermodynamics, Ed. Lawrence L. Quill part of the National Nuclear Energy Series, Manhatten Project Technical Section, Division IV - Plutonium Project Record, Volume 19B, McGraw-Hill Book Co., Inc., New York, 1950.

66. F. H. Spedding and C. F. Miller, J. Am. Chem. Soc. 74, 4195 (1952).

67. G. N. Lewis and M. Randall, revised by K. S. Pitzer and L. Brewer, Thermodynamics, McGraw-Hill Book Company, Inc., New York, 1961.

TECHNICAL INFORMATION DIVISION
LAWRENCE RADIATION LABORATORY
UNIVERSITY OF CALIFORNIA
BERKELEY, CALIFORNIA 94720